JETP Letters, Vol. 74, No. 8, 2001, pp. 405–407. Translated from Pis'ma v Zhurnal Éksperimental'noĭ i Teoreticheskoĭ Fiziki, Vol. 74, No. 8, 2001, pp. 445–447.

Possibility of Precision Experimental Verification of Time Retardation in Moving Clocks by Using Coherent Excitation of Relativistic Nuclei in a Crystal

V. V. Okorokov

Institute of Theoretical and Experimental Physics, ul. Bol'shaya Cheremushkinskaya 25, Moscow, 117218 Russia
e-mail: okorokov@vxitep.itep.ru

Received December 29, 2000; in final form, September 25, 2001

Experiments with coherent excitation of relativistic nuclei in a crystal are proposed to investigate Lorentz time retardation. At present, these experiments provide the possibility of precisely (10^{-4}–10^{-5}) verifying time retardation for clock velocities corresponding to the Lorentz factor $\gamma \sim 100$–200 and larger. © *2001 MAIK "Nauka/Interperiodica".*

PACS numbers: 24.30.Gd; 03.30.+p

A nucleus (or atom) moving in a spatially periodic crystal field is exposed to time-periodic perturbation, whose frequency depends on the nucleus velocity ν as

$$\nu = v/a,$$

where a is the interatomic spacing in the crystal. Because the electric field of the crystal is not purely sinusoidal, the electromagnetic perturbation acting on the moving nucleus includes, along with the fundamental frequency ν, many harmonics:

$$kv/a,$$

where $k = 1, 2, 3, \ldots$. If one of these frequencies coincides with the transition frequency to the excited state of a moving nucleus, the probability of exciting this nucleus sharply increases:

$$\nu_{exc} = \Delta E/h = kv/a \quad (1)$$

where $\Delta E = E_{exc} - E_{gr}$ is the nuclear excitation energy. Such a transformation of the spatially periodic crystal field (in general, it need not necessarily be a crystal) into a time-periodic electromagnetic perturbation acting on a nucleus moving through the crystal and the simultaneous use of this periodic perturbation for the excitation of internal degrees of freedom of the moving nucleus was called coherent excitation [1, 2].[1] This excitation is virtually similar to nuclear excitation by the periodic field of a monochromatic electromagnetic wave, whose frequency coincides with the transition frequency between nuclear levels. Although the coherent excitation (CE) was recently extensively studied both experimentally [3–10] and theoretically [11–22], I think that the direction of these works falls far short of providing complete use of the scientific potentials of CE for fundamental studies. In particular, the experimental observation of the CE of relativistic nuclei in a crystal (the existence of this effect has never been doubted theoretically) will mean the discovery of a nuclear reaction of a new type occurring not in single collisions of two particles but by virtue of the collective interaction between a nucleus moving through crystal and the crystal atoms. The probability of this reaction should be appreciably higher (by a factor of 10^4–10^5) than the probability of an ordinary Coulomb excitation of a nuclei moving through an isotropic target [2], and it should exhibit resonance dependence on the nuclear energy (the relative half width $\Delta E/E$of the resonance can be as small as 10^{-5}). These features provide numerous and promising possibilities of employing this phenomenon in fundamental studies on special and general relativity, as well as on relativistic nuclear physics.

One of these interesting and as yet unrealized possibilities of using CE in fundamental research was pointed out in my recent work [21].

The purpose of this work was to adduce additional arguments in favor of the assumption that an experiment (as yet unrealized) on the CE of nuclear levels may provide quite precise verification of time retardation for relativistic,

$$\gamma = \frac{1}{\sqrt{1 - v^2/c^2}} \approx 150\text{–}200,$$

and ultrarelativistic cases. It is the nuclear CE that can yield the most attractive and interesting results.

For the relativistic energies of a nucleus moving through a crystal, Eq. (1) should be written as

$$\frac{\Delta E}{h} = k\frac{1}{a\sqrt{1 - v^2/c^2}} = k\frac{v}{a}\gamma, \quad (2)$$

[1] After work [5], the less appropriate (in my opinion) term "resonant coherent excitation" was also used.)

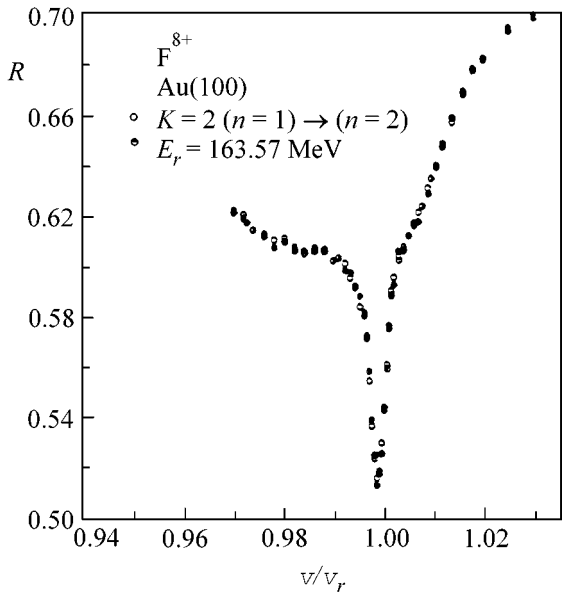

The fraction R of F^{8+} ions passing through a 1600-Å thick Au crystal in the [100] direction vs. the ratio of the F^{8+} velocity to the velocity corresponding to the resonance excitation of the unperturbed 1s–1p transition. The resonance energy is E_r = 163.57 MeV.

where

$$\gamma = \frac{1}{\sqrt{1 - v^2/c^2}}$$

is the Lorentz factor of the particle moving through the crystal.

The γ factor appears because of the relativistic contraction of crystal atoms and interatomic spacings in the frame of reference associated with the moving nucleus. In the crystal frame of reference, the γ factor appears due to the relativistic increase, by a factor of γ, in time intervals in the nuclear frame of reference (i.e., to the decrease, by a factor of γ, in the transition frequency between the levels of moving nucleus).

Therefore, the experimental verification of Eq. (2) provides information about a change in time in the frame of reference moving with a relativistic velocity, which is necessary for the CE of nuclear levels.

In this experiment, a nucleus moving through a crystal and having the $h\nu_{exc} = E_{exc} - E_{gr}$ level represents a moving clock, whose time is checked by a series of sequential interactions of the nucleus with the electric field of atoms located in the sites of a spatially periodic crystal structure.

The probability of coherent Coulomb excitation is noticeable in very narrow mutually well-separated intervals of nuclear velocity (energy) [2]. The positions of these intervals are determined by the nuclear excitation energy and can easily be calculated.

The nuclear energy necessary for the coincidence of one of the collision-frequency harmonics with the transition frequency between the levels of a nucleus colliding with crystal atoms (i.e., for the CE kinematic condition to be fulfilled) can be obtained from Eq. (2):

$$E_{kin} = M_{nucl}c^2\left(\sqrt{\left(\frac{\Delta E a}{hck}\right)^2 + 1} - 1\right), \qquad (3)$$

where $M_{nucl}c^2$ is the nuclear mass measured in MeV's. A quantitative difference between the calculated value of E_{kin} and its experimental value, which may and must be observed in nuclear CE, solves the problem of precision experimental verification of time retardation for the Lorentz factors used in experiments with nuclear beams (e.g., $\gamma \sim$ 150–200 at CERN [23]). The accuracy of verification of Eq. (2) for various Lorentz factors γ is determined only by the relative energy spread in a nuclear beam from an accelerator. The latter can likely be made as small as ~10^{-5} and even smaller by special procedures.

Recall that the natural resolution of the CE of relativistic nuclei in a crystal can easily be made smaller than this value by a mere increase in the number of layers in crystal [1, 2].

A Lorentz factor larger than 200 has long been achieved in the ^{32}S and ^{16}O beams at the CERN accelerator [23]. It may appear, in principle, that the experiments on the CE of atomic levels (see, e.g., [5, 6]) can be used to determine the dependence of the rate of "atomic clock" on the Lorentz factor of the atomic beam. Unfortunately, the numerical factors in Eqs. (2) and (3) are such that the atomic-beam velocities necessary for an experiment on the CE of atomic levels with energies 100–1000 eV correspond to a weakly relativistic case $\gamma \sim$ 1 and, hence, to an unattractive weak change in the rate of atomic clock.

However, of even greater importance is the unavoidable fact that the resonance observed in experiments on the CE of atomic levels is systematically shifted from its calculated value by several fractions of a percent to lower energies (see figure in [20]). This shift is due to the constant component of the crystal electric field, which shifts electronic levels of an atom moving through a medium (Stark effect) [22] and, therefore, impedes precision checking of Eq. (3).

Thus, the precision verification of a relativistic change in time rate (particularly for large Lorentz factor) is possible, in my opinion, only in the experiments with the CE of relativistic nuclei in a crystal (Stark effect is absent for nuclear levels). Such an experiment has, as yet, not been carried out, although it is simple [23, 24] and does not require the fabrication of enormous setups, which are typical for some experiments in high energy physics.

Finally, in light of the positive results obtained in the studies of the atomic CE [3–10], the absence of a simi-

lar CE phenomenon for the relativistic nuclei moving through a crystal is highly improbable.

REFERENCES

1. V. V. Okorokov, Pis'ma Zh. Éksp. Teor. Fiz. **2**, 175 (1965) [JETP Lett. **2**, 111 (1965)].
2. V. V. Okorokov, Yad. Fiz. **2**, 1009 (1965) [Sov. J. Nucl. Phys. **2**, 719 (1965)].
3. V. V. Okorokov, D. L. Tolchenkov, I. S. Khizhnyakov, *et al.*, Pis'ma Zh. Éksp. Teor. Fiz. **16**, 588 (1972) [JETP Lett. **16**, 415 (1972)]; Phys. Lett. A **43A**, 485 (1973).
4. M. J. Gaillard, J. C. Poizat, J. Remillieux, and M. L. Gaillard, Phys. Lett. A **45A**, 306 (1973).
5. S. Datz, C. M. Moak, O. H. Chawford, *et al.*, Phys. Lett. **40**, 843 (1978).
6. C. M. Moak, S. Datz, O. H. Chawford, *et al.*, Phys. Lett. A **19A**, 843 (1979).
7. F. Fujimoto, Nucl. Instrum. Methods Phys. Res. B **40/41**, 165 (1989).
8. Y. Iwata, K. Komaki, Y. Yamazaki, *et al.*, Nucl. Instrum. Methods Phys. Res. B **48**, 163 (1990).
9. I. U. Andersen, G. C. Ball, I. Chevallier, *et al.*, Nucl. Instrum. Methods Phys. Res. B **119**, 292 (1996).
10. S. Datz, P. F. Dittner, H. F. Krause, *et al.*, Nucl. Instrum. Methods Phys. Res. B **100**, 272 (1995).
11. N. P. Kalashnikov and S. G. Pankratov, Fiz. Tverd. Tela (Leningrad) **16**, 843 (1974) [Sov. Phys. Solid State **16**, 542 (1974)].
12. I. Kondo, J. Phys. Soc. Jpn. **36**, 1406 (1974).
13. S. Shindo and Y. H. Ohtsuki, Phys. Rev. B **14**, 3929 (1976).
14. Y. Yamashita and Y. H. Ohtsuki, Phys. Rev. B **22**, 1183 (1980).
15. Yu. L. Pivovarov, A. A. Shirokov, and S. A. Vorob'ev, Dokl. Akad. Nauk SSSR **272**, 86 (1983) [Sov. Phys. Dokl. **28**, 753 (1983)].
16. Yu. L. Pivovarov and A. A. Shirokov, Yad. Fiz. **44**, 882 (1986) [Sov. J. Nucl. Phys. **44**, 569 (1986)].
17. A. Yu. Dubin, Yad. Fiz. **52**, 1243 (1990) [Sov. J. Nucl. Phys. **52**, 790 (1990)].
18. R. Fusina and J. C. Kimball, Nucl. Instrum. Methods Phys. Res. B **27**, 368 (1987).
19. Yu. L. Pivovarov, Nucl. Instrum. Methods Phys. Res. B **145**, 96 (1998).
20. P. D. Miller, H. F. Krause, I. A. Biggerstaff, *et al.*, Nucl. Instrum. Methods Phys. Res. B **13**, 56 (1986).
21. V. V. Okorokov, Pis'ma Zh. Éksp. Teor. Fiz. **62**, 895 (1995) [JETP Lett. **62**, 911 (1995)]; Nucl. Instrum. Methods Phys. Res. B **145**, 96 (1998).
22. O. H. Crawford and R. H. Ritchie, Phys. Rev. A **20**, 1848 (1979).
23. V. V. Okorokov and S. V. Proshin, Preprint ITEP-13 (1980).
24. V. V. Okorokov, Y. L. Pivovarov, A. A. Shirokov, and S. A. Vorobiev, Preprint ITEP-49 (1990).

Translated by R. Tyapaev

JETP Letters, Vol. 74, No. 8, 2001, pp. 408–410. Translated from Pis'ma v Zhurnal Éksperimental'noĭ i Teoreticheskoĭ Fiziki, Vol. 74, No. 8, 2001, pp. 448–450.

Search for *sp* Interference in the Emission of Prompt Neutrons from ^{235}U Fission Induced by Polarized Thermal Neutrons

G. V. Danilyan,* V. A. Krakhotin, V. S. Pavlov, and A. V. Fedorov

Institute of Theoretical and Experimental Physics, ul. Bol'shaya Cheremushkinskaya 25, Moscow, 117259 Russia

**e-mail: danilyan@vitep5.itep.ru*

Received September 6, 2001

Experimental results on a search for the *sp* interference in the angular distribution of prompt neutrons from ^{235}U fission induced by polarized thermal neutrons are presented. The experiment was carried out with the polarized neutron beam from the reactor of the Moscow Engineering Physics Institute. © *2001 MAIK "Nauka/Interperiodica".*

PACS numbers: 24.80.+y; 25.85.Ec; 24.70.+s

In 1998–1999, the collaboration of the ITEP, Universität Tübingen, PNPI, ILL, and Kurchatov Institute culminated in the discovery of the formally *T*-odd correlation that manifests itself in the left–right asymmetry of emitting long-range α particles about the plane specified by the vectors of neutron polarization and light-fragment momentum in ternary fission induced by polarized neutrons [1, 2]. This asymmetry is expressed as

$$W \sim (1 + D_\alpha \mathbf{s}_n[\mathbf{n}_{\rm lf}, \mathbf{n}_\alpha]), \quad (1)$$

where D_α is the correlation coefficient, $\mathbf{s}_n$ is the unit vector along the neutron beam polarization, and $\mathbf{n}_{\rm lf}$ and $\mathbf{n}_\alpha$ are unit vectors along the momenta of the light fragment and α particle, respectively. The asymmetry coefficients not normalized to 100% polarization of fissioning nuclei were found to be on the order of 10^{-3} for $^{233, 235}$U.

There are several possible origins of this correlation. Of course, this may be the manifestation of *T*-noninvariant forces similar to those occurring in the K^0-meson decay. But it is much more probable that this is due merely to the effect of final-state interaction. However, even in this case, the question of which interaction—strong or electromagnetic—is responsible for this effect and why the correlation "survives" after summation over great many final states remains open.

To answer these questions, one should find a process for which one of these interactions is minimal. Measurement of an analogous correlation for the direction of the momentum of a fission neutron rather than of an α particle seems to be most promising. In this case, the process is, likely, similar to ternary fission, but with the emission of an electrically neutral particle, i.e., a neutron. In this process, the electromagnetic interaction in the final state is strongly suppressed, as compared to the ternary fission.

The experimental investigation of this process is complicated because most fission neutrons are emitted from fragments and, therefore, their emission mechanism differs from that for α particles, which are predominantly emitted from the neck region approximately at the scission time, as follows from their angular distribution. In view of this fact, we are interested only in the prescission neutrons, i.e., neutrons emitted through the analogous mechanism rather than from the fragments. Fission neutrons emitted from the fragments form a background, which is very strong in this process and suppresses the desired asymmetry

$$W \sim (1 + D_n \mathbf{s}_{\rm in}[\mathbf{n}_{\rm lf}, \mathbf{n}_{\rm sn}]). \quad (2)$$

where D_n is the correlation coefficient, $\mathbf{s}_{\rm in}$ is the unit vector along the neutron-beam polarization, and $\mathbf{n}_{\rm lf}$ and $\mathbf{n}_{\rm sn}$ are unit vectors along the momenta of the light fragment and prescission neutron, respectively.

Information about the fraction of prescission neutrons among the prompt fission neutrons is very contradictory. Estimates vary from 3 to 35% [3]. At present, not only reliable data on their energy and angular distribution are lacking, but even direct evidence of their existence is not available.

If the prescission neutrons exist, then one may observe triple correlation of a different form

$$W \sim (1 + B \mathbf{s}_n[\mathbf{n}_{\rm in}, \mathbf{n}_{\rm fn}]). \quad (3)$$

where B is the correlation coefficient, $\mathbf{s}_{\rm in}$ is the unit vector along the neutron-beam polarization, and $\mathbf{n}_{\rm in}$ and $\mathbf{n}_{\rm fn}$ are unit vectors along the momenta of the initial and final neutrons, respectively. This correlation is caused

by the interference of *s* and *p* waves in the entrance reaction channel. A similar correlation was observed for the fission fragments and gamma-ray quanta, with the correlation coefficient for the fission induced by thermal neutrons being on the order of 10^{-4}. Therefore, the presence of this correlation may indicate the possibility of existing correlation (2) for the prescission fission neutrons, provided that correlation (1) is not dominated by the electromagnetic interaction in the final state.

Figure 1 shows the scheme of the experiment. The basic unit of the setup is a low-pressure chamber filled with hexane to a pressure of 3 torr. A two-sided target *U* containing 1.3 g of ^{235}U on a thick substrate is placed at the chamber center. The target is irradiated by a beam of polarized neutrons perpendicularly to the figure plane. The neutron polarization **s** is perpendicular to the target plane and changes its direction every second.

Multiwire avalanche detectors, used as fission-fragment detectors *f*, are placed on each side of the target at 2 cm from it.

Neutron detectors *n*1 and *n*2 are placed on each side of the chamber at a distance of 25 cm from the target in the direction perpendicular to the beam axis and spin of incident neutron. Each detector consists of a plastic scintillator and a photomultiplier. Neutrons and gamma-ray quanta detected by neutron detectors are discriminated by the time-of-flight method.

A fission signal arrives from one of the fragment detectors. The same signal triggers time-to-code converters. A signal from the neutron detector is the shut-off signal for the converters. Therefore, the method of delayed coincidences of the fragment signal and the signal from the neutron detectors makes it possible to separate neutrons from gamma-ray quanta.

A typical spectrum of the delay time between the signal from the neutron detector and the signal from the fragment detector is shown in Fig. 2, where two maxima are seen. The left and right maxima are due to gamma-ray quanta and neutrons, respectively.

For analysis, this spectrum is divided into three parts. The first part is the gamma-peak region, the second is the region of neutrons with energies above 0.7 MeV, and the third is for low-energy neutrons. The asymmetry *a* is separately calculated for each part by the formula

$$a = (N_+ - N_-)/(N_+ + N_-), \quad (4)$$

where N_+ and N_- are the numbers of events for different polarization signs of the neutrons incident on the target.

The coefficient *B* in Eq. (3) is determined as

$$B = a/(PCn_s), \quad (5)$$

where *P* is the degree of polarization of the fissioning nuclei, *C* is the mean value of the triple scalar product $\mathbf{s}_n[\mathbf{n}_{in}, \mathbf{n}_{fn}]$ in the geometry of the experiment, and n_s is the ratio of the number of prescission neutrons to the total number of prompt fission neutrons.

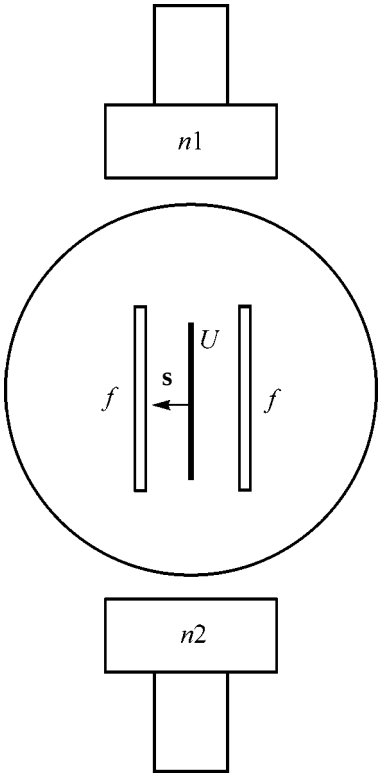

Fig. 1. The scheme of the set.

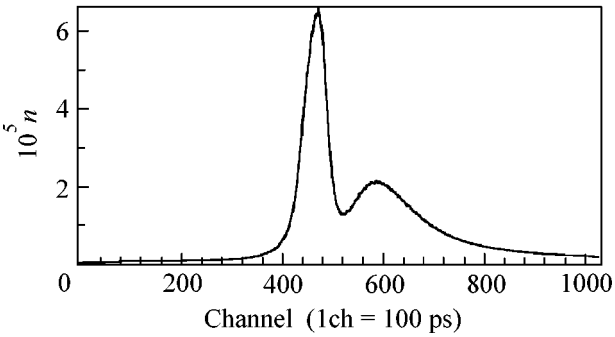

Fig. 2. Time-of-flight spectrum.

The results are as follows.

Group of events:	asymmetry *a*, 10^5
Gamma-ray quanta:	$+0.8 \pm 2.2$
High-energy neutrons:	-9.4 ± 3.0
Low-energy neutrons:	-6.8 ± 2.9

The result obtained for neutrons with energies above 0.7 MeV exceeds three errors, which is surprising for us because prescission neutrons should be softer than neutrons emitted from the fragments. However, if this asymmetry was instrumental, it would be manifested in the photon asymmetry as well. It is worthwhile carrying out similar measurements in the resonance region of neutron energy because the *sp*-interference effects for the fission fragments are considerably larger in resonances.

We are grateful to the staff of the reactor at Moscow Engineering Physics Institute for assistance and to Yu.A. Belov, our technician.

This work was supported by the Russian Foundation for Basic Research, project no. 00-02-16011.

REFERENCES

1. P. Jesinger, G. V. Danilyan, A. M. Gagarski, *et al.*, Yad. Fiz. **62**, 1723 (1999) [Phys. At. Nucl. **62**, 1608 (1999)].
2. G. V. Danilyan, A. V. Fedorov, A. M. Gagarski, *et al.*, Yad. Fiz. **63**, 1759 (2000) [Phys. At. Nucl. **63**, 1671 (2000)].
3. N. V. Kornilov, A. V. Kagalenko, and F.-J. Hambsch, *New evidence of scission neutron existence*, ISINN-7, Dubna, 1999, p. 241.

Translated by R. Tyapaev

JETP Letters, Vol. 74, No. 8, 2001, pp. 411–414. From Pis'ma v Zhurnal Éksperimental'noĭ i Teoreticheskoĭ Fiziki, Vol. 74, No. 8, 2001, pp. 451–454.

Nuclear Stochastic Resonance[1]

V. P. Berezovoj[1], Yu. L. Bolotin[1]*, A. P. Dzyubak[1], V. V. Yanovsky[1, 2], and A. V. Zhiglo[1]

[1] *National Scientific Center "Kharkov Institute of Physics and Technology," Kharkov, 61108 Ukraine*

**e-mail: bolotin@kipt.kharkov.ua*

[2] *Institute of Single Crystals, National Academy of Sciences of Ukraine, Kharkov, 61001 Ukraine*

Received September 13, 2001

Fission decay of highly excited periodically driven compound nuclei is considered in the framework of the Langevin approach. We used residual-time distribution (RTD) as a tool for studying dynamic features in the presence of periodic perturbation. The structure of RTD essentially depends on the relation between Kramers' decay rate and the frequency ω of periodic perturbation. In particular, the intensity of the first peak in RTD has a sharp maximum at certain nuclear temperature depending on ω. This maximum should be considered as first-hand manifestation of stochastic resonance in nuclear dynamics. *© 2001 MAIK "Nauka/Interperiodica".*

PACS numbers: 25.85.-w; 05.45.Xt

Since its discovery, the atomic nucleus has been constantly used for verifying new physical ideas such as tunneling [1], superfluids [2], superconductivity [3], supersymmetry [4], and dynamical chaos [5]. Thus, it seems unnatural that one of the most recent and intriguing discoveries in nonlinear physics—stochastic resonance (SR) (see [6] for a recent review)—has still not found response of the nuclear community. This is particularly strange because there is no doubt that the theory in collective nuclear motion claiming to be a consistent description of nuclear dynamics must essentially be a nonlinear theory. The aim of this work is to demonstrate the possibility of the observation of SR in nuclear dynamics. As a specific example, we consider the process of induced nuclear fission in the presence of weak periodic perturbation.

SR was introduced nearly 20 years ago to explain the periodicity of the Earth's ice ages [7, 8] and found numerous applications in such diverse fields as physics, chemistry, and biology (see [6]).

The mechanism of SR can be explained in terms of the motion of a particle in a symmetric double-well potential subjected to noise and time periodic forcing. The noise causes incoherent transitions between two wells with a well-known Kramers' rate [9] r_k. If we apply a weak periodic forcing, noise-induced hopping between the potential wells can become synchronized with the periodic signal. This statistical synchronization takes place under the condition

$$r_k^{-1} \approx \pi/\omega, \qquad (1)$$

where ω is the frequency of periodic forcing. Two prominent feature of SR arises from synchronization condition (1):

(i) the signal-to-noise ratio does not decrease monotonically with increasing noise amplitude (as it happens in linear system), but attains a maximum at a certain noise strength [optimal noise amplitude can be found from Eq. (1), because r_k is simply connected with it];

(ii) the residence-time distribution (RTD) demonstrates a series of peaks, centered at odd multiples of half driving period $T_n = 2\left(n - \frac{1}{2}\right)\frac{\pi}{\omega}$ with exponentially decreasing amplitude. Notice that if a single escape from a local potential well is the event of interest, then RTD reveals the dynamics of the considered system more transparently than the signal-to-noise ratio. These signatures of SR are not confined to the special models but occur in general bi- and monostable systems and for different types of noise [6].

Kramers [9] was the first to consider nuclear fission as a process of overcoming the potential barrier by a Brownian particle. A slow fission degree of freedom (with large collective mass) is considered as the Brownian particle, and fast nucleon degrees of freedom are considered as a heat bath. The adequacy of such a description is based on the assumption that the time of equilibrium achievement in the system of nucleon degrees of freedom is much less than the characteristic time scale of collective motion. The most general way of describing dissipative nuclear dynamics is through the Fokker–Planck equation [10]. However, for the demonstration of qualitative effects, it is convenient to use the Langevin equation [11], which is equivalent to the Fokker–Planck equation but is more transparent. As has been shown, the description based on the Langevin equation adequately represents nuclear dissipative phenomena such as heavy-ion reactions and fission decay [12–14] and possesses a number of advantages over the Fokker–Planck description.

[1] This work was submitted by the authors in English.

0021-3640/01/7408-0411$21.00 © 2001 MAIK "Nauka/Interperiodica"

Since we only intend to qualitatively demonstrate SR in a nucleus, let us consider the simplest type of Langevin equation: one-dimensional problem with inertial M and friction γ parameters independent of coordinates. The fission coordinate R is considered as a coordinate of the Brownian particle. The remaining degrees of freedom act as the heat bath. The interaction of the fission coordinate with this heat bath causes a friction γP and a random force $\xi(t)$.

The particle motion in the presence of an external periodic force $A\cos\omega t$ is described by the Langevin equation for canonically conjugate variables $\{P, R\}$

$$\begin{aligned} dR/dt &= P/M, \\ dP/dt &= -\beta P = dV/dR + A\cos(t) + \xi(t); \\ \beta &= \gamma/M, \end{aligned} \tag{2}$$

$\xi(t)$ is stochastic force possessing statistical properties of white noise:

$$\begin{aligned} \langle \xi(t) \rangle &= 0, \quad \langle \xi(t)\xi(t') \rangle = 2D\delta(t-t'), \\ D &= \gamma T. \end{aligned} \tag{3}$$

The nuclear temperature $T(\mathrm{MeV}) = \sqrt{E^*/a}$, where E^* is an excitation energy and the level-density parameter $a = \tilde{A}/10$ ($\tilde{A}$ is a mass number). The deformation potential V is given as [12]

$$V(R) = \begin{cases} 37.46(R-1)^2(\mathrm{MeV}), & 0 < R < 1.27 \\ 8.0 - 18.37(R-1.8)^2(\mathrm{MeV}), & R > 1.27 \end{cases} \tag{4}$$

(these are the parameters of ^{205}At nucleus [12]).

Plausible sources of periodic perturbation are considered below.

The discretized form of the Langevin equation is given by [13, 14]

$$\begin{aligned} R_{n+1} &= R_n + \tau\frac{P_n}{M}, \\ P_{n+1} &= P_n(1-\beta\tau) \\ &- \left[\left(\frac{dV(R)}{dR}\right)_n + A\cos t_n\right]\tau + \sqrt{\frac{2\beta MT\tau}{N}}\eta(t_n). \end{aligned} \tag{5}$$

Here, $t_n = n\tau$ and $\eta(t_n)$ is the normalized Gaussian-distributed random variable which satisfies

$$\langle \eta(t) \rangle = 0, \quad \langle \eta(t_n)\eta(t_{n'}) \rangle = N\delta_{nn'}. \tag{6}$$

The efficiency of numerical algorithm (5) was checked for the following cases:

(i) $V = 0$, $A = 0$, where numerical and analytical results for $\langle P^2 \rangle$ and $\langle R^2 \rangle$ can be compared [12];

(ii) $V \neq 0$, $A = 0$, where numerical and analytical values for Kramers' decay rate r_k can be compared. According to [9],

$$\begin{aligned} r_k &= \frac{\omega_{\min}}{2\pi}[\sqrt{\tilde{\beta}^2 + 1} - \tilde{\beta}]\exp(-\Delta V/T) \equiv W\exp(-\Delta V/T), \\ \tilde{\beta} &= \frac{\beta}{2\omega_{\max}}. \end{aligned} \tag{7}$$

Here, $\omega_{\min}$ and $\omega_{\max}$ are the angular frequencies of potential (4) at the potential minimum and at the top of barrier, respectively, and ΔV is the height of the potential barrier. Numerical values of Kramers' decay rates r_k^i for the time bin i are calculated by sampling the number of fission events $(N_f)_i$ in the ith time-bin width Δt and normalizing to the number of nuclei $N_{\mathrm{total}} - \sum_{j<i}(N_f)_j$ which have not fissioned,

$$r_k^i = \frac{1}{N_{\mathrm{total}} - \sum_{j<i}(N_f)_j}\frac{(N_f)_i}{\Delta t}. \tag{8}$$

The comparison of Eq. (7) with the asymptotic value of Eq. (8) was used for the determination of the time interval τ, which provides saturation for numerical integration (5). From the results, one could see that 20 steps per nuclear time $\hbar$/MeV provides a good saturation.

Now let us proceed to the description of the expected effect—the manifestation of SR in nuclear fission. For the usually considered case of a symmetric double well in the absence of periodic forcing, RTD $N(t)$ has the exponential form (see [6]) $N(t) \sim \exp(-r_k t)$. In the presence of the periodic forcing, one observes a series of peaks centered at odd multiples of the half driving period $T_\omega = 2\pi/\omega$. The heights of these peaks decrease exponentially with their order number.

These peaks can be simply explained [15]. The best time for the particle to escape the potential well is when the potential barrier becomes minimum. Thus, $t = 1/2T_\omega$ is a preferred residence time interval. The next "good opportunity" to escape occurs after a full period, when the potential barrier achieves its minimum again. The second peak in the RTD is therefore located at $3/2T_\omega$. The location of the other peaks is evident. The peak heights decay exponentially, because the probabilities of a particle jumping over a potential barrier are statistically independent. As shown for a symmetric double-well potential [16], the strength P_1 of the first peak at $1/2T_\omega$ (the area under peak) is a measure of the synchronization between the periodic forcing and the switching between the wells. So, if the mean residence time (MRT) of the particle in one potential well is much larger than the period of driving, the particle is not likely to jump at the first time the relevant potential barrier becomes minimum. In such a case, the RTD exhibits a larger number of peaks, where P_1 is small. If the

MRT is much shorter than the period during which the driving RTD decays practically to zero before the time $1/2T_\omega$ is reached, the weight P_1 is again small. Optimal synchronization, i.e., maximum P_1, is reached when the MRT matches the half driving period, i.e., condition (1). This resonance condition can be achieved by varying the noise intensity D (or ω).

For constructing RTD (and following P_1 calculation), we use the numerical solutions of Langevin Eq. (5). We studied the evolution of P_1 within the temperature interval 1 MeV $\le T \le$ 6 MeV. Let us fix the frequency of periodic perturbation ω = 0.0267 MeV/$\hbar$ ($T_\omega/2 \approx 117.7\ \hbar$/MeV), which is the resonant frequency at T = 3 MeV [following Eq. (1)]. The results of numerical procedure for RTD under fixed parameters of periodic perturbation [A = 3, ω = 0.0267; determined from resonance condition (1)] are presented in Fig. 1. Nuclear friction β in all numerical calculation is chosen to be 1 MeV/$\hbar$.

In accordance with the expected behavior at T = 1 MeV (for low r_k), one can distinctly see three peaks located near $t = T_\omega/2$(~117.7), $3/2T_\omega$(~353), and $5/2T_\omega$(~588); and at T = 4 MeV almost all RTD is concentrated near t = 0 (with width less than $T_\omega/2$). The corresponding variations of P_1 (which represents the measure of synchronization between the periodic forcing and Kramers' transitions and, hence, the measure of SR) are depicted in Fig. 2 for two frequencies of periodic perturbation [corresponding to temperatures 2 and 3 MeV from Eq. (1)]. Maxima of intensities P_1 are close to the predicted values of temperature.

The above-calculated P_1 can be estimated theoretically for a single-well situation using a model similar to the two-states model [6].

Let us evaluate RTD for the single-well case. The rate equation for the number of fissile nuclei should be written as

$$\frac{dn}{dt} = -nr_k e^{-\epsilon\cos\omega t}, \tag{9}$$

where $\epsilon = A/T$. At low temperature, Eq. (9) properly describes the process modeled below (though it is inappropriate at T comparable with ΔV, when r_k is not much smaller than the relaxation time within the well). The solution to Eq. (9) is

$$\ln\frac{n(t)}{n_0} = -r_k\int_0^t \exp(-\epsilon\cos\omega t)\,dt$$
$$= -r_0 t + \sum_{n=1}^{\infty}(-1)^n I_n(\epsilon)\frac{2r_k}{n\omega}\sin n\omega t, \tag{10}$$

where $r_0 = r_k I_0(\epsilon) > r_k$; $I_n(\epsilon)$ are the modified Bessel functions. RTD in this model is given by $N(t) = -dn/dt$, so that

$$N(\pi/\omega) = r_k\exp(-r_0\pi/\omega + \epsilon). \tag{11}$$

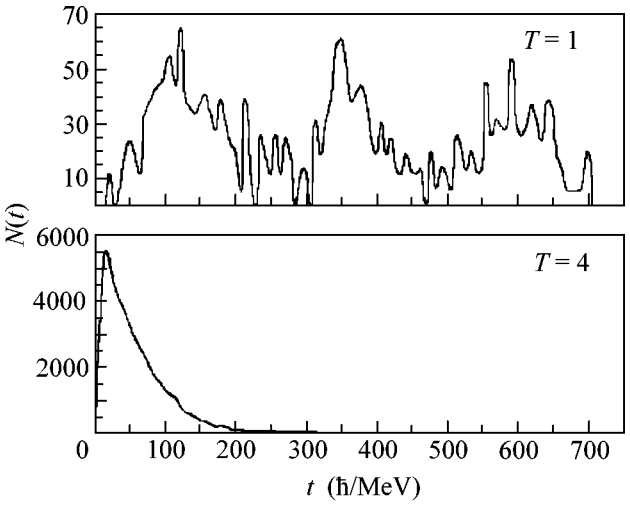

Fig. 1. RTD for T = 1 and T = 4.

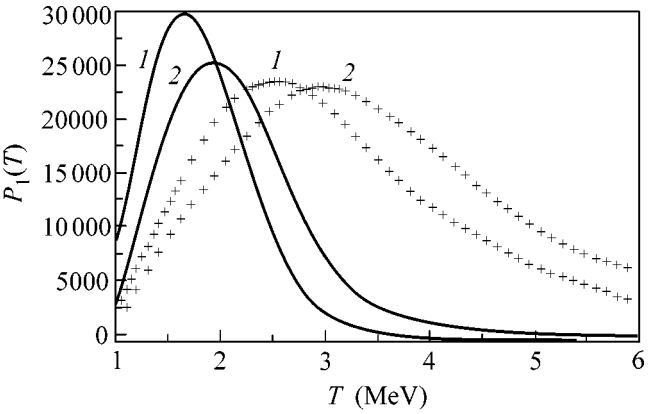

Fig. 2. $P_1(T)$ at ω = 0.0267 (crosses) and ω = 0.007 (solid); *1* corresponds to Eq. (12) and *2* is for the numerical calculation.

Using Eqs. (9)–(11), we obtain the new condition for resonant temperature $T_{RES}(\omega)$, which provides the maximal value for $N(\pi/\omega)/\omega$, whose dependence on ω and T properly represents $P_1(\omega, T)$ calculated above:

$$r_k^{-1} = \frac{\pi}{\omega}\frac{\lambda I_0(\epsilon) - I_1(\epsilon)}{\lambda - 1}, \tag{12}$$

instead of Eq. (1); $\lambda = \Delta V/A$. The numerical solution to Eq. (12) for $T_{RES}(\omega)$ is presented in Fig. 3 [together with a solution to

$$r_k^{-1} = 2\pi/\omega, \tag{13}$$

which approximates curve (12) much better than 1].

$P_1(T)$ [obtained from Eq. (11)] depicted in Fig. 2 is to be compared with numerical results; the scale of

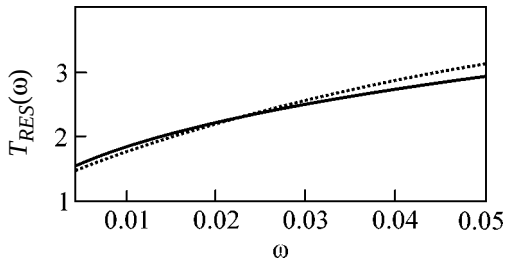

Fig. 3. Resonant conditions (12) and (13) for $T_{RES}(\omega)$.

$P_1(T)$ is chosen in such a way that the height of (12) in its maximum for $\omega = 0.0267$ coincides with the numerical data. Higher resonant T in the latter case is connected with nonequilibrium distribution within a long interval near $t = 0$ (which can be easily seen in Fig. 1).

The first maximum in RTD is shifted from π/ω, so it may seem more reasonable to evaluate the height in true maximum. The calculation shows that this height dependence on ω resembles that presented in Fig. 3, with the exception of the region of high T, where the curve $N(t)$ does not possess any maxima. Nevertheless, $N(\pi/\omega)$ is easily defined and observable, and studying its dependence on T allows one to determine the necessary characteristics of the nucleus.

In conclusion, let us briefly consider the possible sources of periodic perturbation. The first possibility is the fissile nucleus as a component of the double nuclear system formed, for example, in heavy-ion collisions [17]. In this case, the deformation potential will experience periodic perturbation similar to tide waves on the Earth caused by the Moon's rotation. In the case of asymmetric fission, an alternating electric field may be the source of periodic perturbation. The problem of the choice of periodic perturbation should be discussed separately.

We thank A.Yu. Korchin for valuable discussions.

REFERENCES

1. G. Gamow, Z. Phys. **51**, 204 (1928).
2. A. Bohr, B. Mottelson, and D. Pines, Phys. Rev. **110**, 936 (1958).
3. S. T. Belyaev, K. Dan. Videns. Selsk. Mat. Fys. Medd. **31**, 11 (1959).
4. F. Iachello, Phys. Rev. Lett. **44**, 772 (1980).
5. Yu. L. Bolotin and I. V. Krivoshey, Yad. Fiz. **42**, 53 (1985) [Sov. J. Nucl. Phys. **42**, 32 (1985)].
6. L. Gammaitoni, P. Hänggi, P. Jung, and F. Marchesoni, Rev. Mod. Phys. **70**, 223 (1998).
7. R. Benzi, A. Sutera, and A. Vulpiani, J. Phys. A **14**, L453 (1981).
8. C. Nicolis, Tellus **34**, 1 (1982).
9. H. A. Kramers, Physica (Amsterdam) **7**, 284 (1940).
10. H. Risken, *The Fokker-Planck Equation* (Springer-Verlag, Berlin, 1982).
11. P. Langevin and C. R. Hebd, Seances Acad. Sci. **146**, 530 (1908).
12. Y. Abe, C. Gregoire, and H. Delagrange, J. Phys. (Paris) **47**, 329 (1986).
13. Y. Abe, S. Ajik, P.-G. Reinhard, and E. Suraud, Phys. Rep. **275**, 49 (1986).
14. P. Frobrich and I. I. Gontchar, Phys. Rep. **292**, 131 (1998).
15. T. Zhou, F. Moss, and P. Jung, Phys. Rev. A **42**, 3161 (1990).
16. L. Gammaitoni, F. Marchesoni, and S. Santucci, Phys. Rev. Lett. **74**, 1052 (1995).
17. V. V. Volkov, *Nuclear Reactions of Deep Inelastic Transfers* (Énergoizdat, Moscow, 1982).

JETP Letters, Vol. 74, No. 8, 2001, pp. 415–417. Translated from Pis'ma v Zhurnal Éksperimental'noĭ i Teoreticheskoĭ Fiziki, Vol. 74, No. 8, 2001, pp. 455–457.

Hybridization of Libron and Phonon Modes in NH_4I: Neutron Spectroscopy Studies at Pressures up to 10 GPa

V. P. Glazkov[1], D. P. Kozlenko[2], B. N. Savenko[2], V. A. Somenkov[1], and A. S. Telepnev[2, 3]

[1]*Kurchatov Institute Russian Research Centre, pl. Kurchatova 1, Moscow, 123182 Russia*

[2]*Joint Institute for Nuclear Research, Dubna, Moscow region, 141980 Russia*

[3]*Institute of High-Pressure Physics, Russian Academy of Sciences, Troitsk, Moscow region, 142092 Russia*

Received September 7, 2001

Vibrational spectra of ammonium iodide NH_4I were studied at pressures up to 10 GPa by incoherent inelastic neutron scattering. The pressure dependences of the frequencies of librational and transverse optical modes suggest that they are hybridized upon pressure buildup. © *2001 MAIK "Nauka/Interperiodica".*

PACS numbers: 33.20.Tp; 33.20.Fb; 61.12.Ex; 62.50.+p; 63.20.Dj

High-pressure studies of ammonium halides are of interest for the elucidation of interplay between the structural and dynamical changes and phase transitions occurring upon a decrease in volume [1]. The influence of high pressure on the librational mode of ammonium ions and the phase-transition-induced changes in its behavior are among the most intriguing aspects of the dynamics of ammonium halides [2].

The vibrational spectra of NH_4I have been studied by neutron spectroscopy at pressures below 4.5 GPa [3] and by Raman spectroscopy at pressures up to 40 GPa [4, 5]. The methods of optical spectroscopy are weakly sensitive to the librational mode because only its overtones and combination frequencies are optically active. By contrast, neutron spectroscopy allows the direct experimental determination of the positions of librational and phonon peaks, though with lower resolution and in a more restricted pressure range. At pressure $P \sim 5.5$ GPa, the frequencies in the Raman spectra of NH_4I and ND_4I change substantially, suggesting the appearance of a new high-pressure phase [4]. Considering that the structure of NH_4I at room temperature and pressures above 0.05 GPa is of the CsCl type, where the ammonium ions are orientationally disordered over two equivalent positions [6], it is natural to assume that this new phase is orientationally ordered, as in other ammonium halides. Indeed, the transition to phase V was observed in the neutron diffraction study of ND_4I at substantially higher pressures $P \sim 8$ GPa [7]. It was shown that phase V has the trigonal structure, where the ammonium ions are oriented antiparallel to each other. It was pointed out in [3] that the transition to phase V may be due to the coupling between the transverse optical and librational modes in NH_4I (ND_4I), because the difference between their frequencies decreases with pressure buildup and becomes $\Delta \approx 11$ meV at $P \sim 4$ GPa. To verify this assumption and elucidate the nature of anomalies in the optical spectra, it is necessary to carry out neutron spectroscopic studies of the vibrational spectra of NH_4I above and below the transition pressure, i.e., in the pressure range where the experiments have not been carried out before. In this work, we have attempted to fill this gap using a small-sized autonomous large-aperture press devised for the neutron diffraction experiments by S.M. Stishov and Yu.A. Sadkov at the Institute of High-Pressure Physics, Russian Academy of Sciences.

Experiments were performed at room temperature on a DN-12 spectrometer [8] and pulsed IBR-2 high-flow reactor at the Laboratory of Neutron Physics of the Joint Institute for Nuclear Research (Dubna). Pressure was produced in a high-pressure chamber with double-torus tungsten carbide anvils [9]. The sample volume was 100 mm^3 in the chamber and 60 mm^3 in the zone of neutron beam. The pressure in the chamber was determined from the well-known equation of state for NH_4I [10] and a change in the unit cell parameter, which was measured in the additional diffraction experiments. The energy transfer was analyzed using a beryllium filter set at a scattering angle $2\theta = 90°$. The final energy of detected neutrons was $E = 4$ meV. The measurement time for one spectrum was typically 50 h.

A typical spectrum of the generalized density $G(E)$ of vibrational states of NH_4I at high pressures shows two peaks corresponding to the transverse optical (*TO*) and librational (*L*) modes (inset in Fig. 1). The pressure buildup in the range 0–4 GPa brings about almost linear increase in the *TO* and *L* frequencies with simultaneous decrease in the difference between them. On further pressure increase, the slopes of the corresponding curves change and the difference between the frequencies reaches a minimum $\Delta \approx 9.6$ meV at $P \sim 6$ GPa, after which it again starts to increase (Fig. 2). The Grüneisen parameters $\gamma_i = -d(\ln\nu_i/d\ln V)_T$ for the *TO* and *L* modes

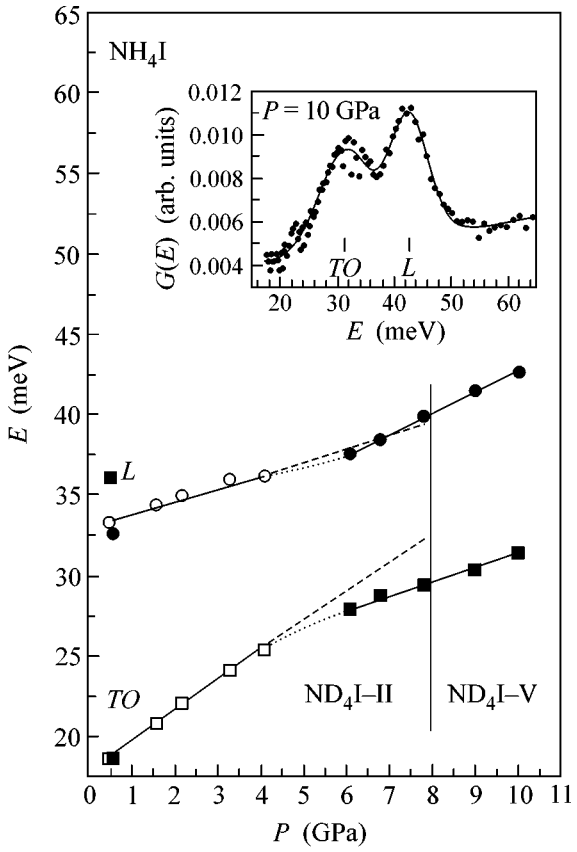

Fig. 1. Pressure dependence of the *L* and *TO* modes of NH_4I. Solid lines are the linear interpolations of experimental data in the ranges 0–4 and 6–10 GPa, respectively; dotted lines are the interpolation in the range 4–6 GPa; and dashed lines are the linear interpolation to the II–V phase-transition point in ND_4I. Black circles and squares are the data of this work; white circles and squares are the neutron data [3]. Inset: generalized density of vibrational states in NH_4I at 10 GPa. The peaks are approximated by Gaussians, and the background, by linear polynomials.

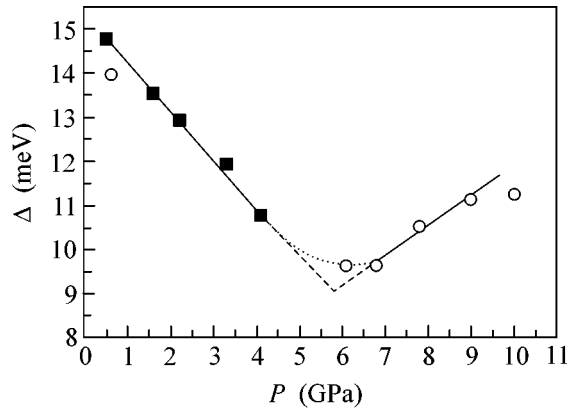

Fig. 2. Pressure dependence of the difference between the frequencies of the *L* and *TO* modes. White circles are the data of this work, and black squares are the data from [3]. In the ranges 0–4 and 7–10 GPa, the experimental data are interpolated by linear functions.

in different pressure ranges are given in the table. The calculations were carried out with the following values of bulk modulus:

$$B(P = 0.5\ \text{GPa}) = 16.8\ \text{GPa},$$

$$B(P = 6.1\ \text{GPa}) = 33.3\ \text{GPa [4]}.$$

It follows from the table and Fig. 2 that the crossover at $P = 6$ GPa corresponds not to the phase transition but to the point where the frequencies of the optical and librational modes "exchange" their derivatives with respect to pressure.

The behavior of the *L* and *TO* frequencies is evidence for the appearance of interaction between them, i.e., for the libron–phonon hybridization. This effect results in the successive attraction and repulsion of the vibrational branches and, respectively, in sizable changes of the Grüneisen parameters: increase in γ_L from 0.4 to 1.2 and decrease in γ_{TO} from 1.7 to 1.0 (table). The nature of this phenomenon is, likely, similar to the hybridization of other types of excitations, in particular, magnons and phonons in magnetic crystals [11]. To every ammonium ion there can be related an orientation vector directed from the center of the NH_4^+ tetrahedron to one of its vertices. The librations are caused by the oscillations of the orientation vectors about their equilibrium positions, much as the atomic magnetic moments oscillate in magnons. However, there are no spatial correlations between the librations of neighboring NH_4^+ ions, so that this branch is virtually dispersionless. In addition, in the disordered phase II, the ammonium ions can execute reorientational jumps between the equivalent positions in the structure [12]. Taking into account that the librational branch is dispersionless and that the dispersion of the optical branch is small, one may assume that the interaction of these branches occurs over a wide range of wave vectors in the Brillouin zone (including its boundaries), and, as a result, it manifests itself in the vibrational density of states. It is conceivable that this is precisely the reason why a superstructure with antiparallel orientations of ND_4I (phase V) appears, in contrast to the parallel superstructures in other ammonium halides. Note that the libron–phonon hybridization is accompanied by the "exchange" not between the positions of interacting branches but between their derivatives with respect to pressure.

The pressure $P \sim 6$ GPa at which the *L* and *TO* modes interact is close to the value $P \sim 5.5$ GPa at which the Raman spectra of NH_4I show appreciable changes [5]. It is not improbable, hence, that the analogous changes in other ammonium halides are also associated with the mode coupling and may precede phase transitions in these systems at higher pressures. To elucidate the role of these interactions in the phase transitions and the hybridization mechanism, it is necessary to experimentally study the dispersion curves at high

Grüneisen parameters for the *L* and *TO* modes of NH_4I

Mode	*P*, GPa	$d\nu_i/dP$, meV/Gpa	γ_I
L	0.5–5 [4]	0.82	0.4(1)
L	6–10	1.32	1.2(2)
TO	0.5–5 [4]	1.89	1.7(2)
TO	6–10	0.85	1.0(1)

pressures and carry out particular calculations by invoking symmetry analysis.

We are grateful to V.L. Aksenov and S.M. Stishov for helpful discussions and assistance in the work. This work was supported by the program "Neutron Studies of Condensed Media" and the Russian Foundation for Basic Research, project no. 00-02-17199.

REFERENCES

1. V. P. Glazkov, D. P. Kozlenko, B. N. Savenko, *et al.*, Kristallografiya **44**, 55 (1999) [Crystallogr. Rep. **44**, 50 (1999)].
2. A. M. Balagurov, B. N. Savenko, A. V. Borman, *et al.*, High Press. Res. **14**, 55 (1995).
3. V. P. Glazkov, D. P. Kozlenko, B. N. Savenko, and V. A. Somenkov, Zh. Éksp. Teor. Fiz. **117**, 362 (2000) [JETP **90**, 319 (2000)].
4. A. M. Heyns, K. R. Hirsch, and W. B. Holzapfel, J. Chem. Phys. **73**, 105 (1980).
5. S. J. Jeon, R. F. Porter, and A. L. Ruoff, J. Raman Spectrosc. **19**, 179 (1988).
6. N. G. Parsonage and L. A. K. Staveley, *Disorder in Crystals* (Clarendon, Oxford, 1978; Mir, Moscow, 1982), Vol. 1.
7. D. P. Kozlenko, V. P. Glazkov, B. N. Savenko, *et al.*, High Press. Res. **17**, 235 (2000).
8. V. L. Aksenov, A. M. Balagurov, V. P. Glazkov, *et al.*, Physica B (Amsterdam) **265**, 258 (1999).
9. L. G. Khvostantsev, L. F. Vereshchagin, and A. P. Novikov, High Temp.- High Press. **9**, 637 (1977).
10. O. Schulte and W. B. Holzapfel, High Press. Res. **4**, 321 (1991).
11. Yu. A. Izyumov and N. A. Chernoplekov, in *Neutrons and Solid*, Vol. 3: *Neutron Spectroscopy*, Ed. by R. P. Ozerov (Énergoatomizdat, Moscow, 1983), p. 115.
12. D. P. Kozlenko, S. Lewicki, J. Wasicki, *et al.*, Mol. Phys. **99**, 427 (2001).

Translated by V. Sakun

JETP Letters, Vol. 74, No. 8, 2001, pp. 418–421. From Pis'ma v Zhurnal Éksperimental'noĭ i Teoreticheskoĭ Fiziki, Vol. 74, No. 8, 2001, pp. 458–461.

Anomalous Resistivity of Lithium at High Dynamic Pressure[1]

V. E. Fortov[1],* V. V. Yakushev[2], K. L. Kagan[2], I. V. Lomonosov[2], V. I. Postnov[2], T. I. Yakusheva[2], and A. N. Kuryanchik[2]

[1] *High Energy Density Research Center, Joint Institute for High Temperatures, Russian Academy of Sciences, ul. Izhorskaya 13/19, Moscow, 127412 Russia*

**e-mail: fortov@ras.ru*

[2] *Institute of Energy Problems of Chemical Physics, Chernogolovka branch, Russian Academy of Sciences, Chernogolovka, Moscow region, 142432 Russia*

Received September 7, 2001

The experimental investigation of lithium compressed by multiple shock waves to a pressure of 210 GPa demonstrates the abnormal dependence of electrical resistivity. Contrary to normal metal behavior, the resistivity monotonically increases in the pressure range 30–150 GPa by more than 15 times from a typical metallic value at ambient conditions and reverts to a metallic value at a pressure higher than 160–210 GPa. The obtained results demonstrate the anomalous resistivity of lithium both in solid and in liquid states. © *2001 MAIK "Nauka/Interperiodica".*

PACS numbers: 71.20.Dg; 62.50.+p

High-pressure studies play an important role in understanding fundamental physical properties of condensed matter. The conventional point of view in condensed-matter physics [1] predicts that, as density and pressure increase, structural phase transitions occur in a solid, a closest-packed phase with the maximal coordination number appears, insulators become conductors, and pressure-induced ionization effect takes place under extreme conditions. Numerous experiments and theoretical models seem to support this general picture. Lithium, like other alkali metals, has long been considered as a prototype "simple" metal with metallic bonding. At ambient conditions, alkali metals occur in simple body-centered-cubic or close-packed lattices. But modern sophisticated quantum mechanical calculations by Neaton and Ashcroft [2] predict much more reach and interesting behavior of matter at high pressure. The theory [2] shows that lithium under pressure transforms from a typical metal at ambient pressure to an orthorhombic phase at 50 GPa. At higher pressure, lithium nuclei form pairs, producing a molecular semimetallic structure near 100 GPa, and finally revert to a monoatomic metal at very high pressures. Preliminary experiments carried out in diamond anvil cells [3, 4] to a pressure of 60 GPa have demonstrated a number of interesting optical anomalies, but they did not deal with measurements of electrical resistivity—the main indicator of metal–insulator transitions. Recent X-ray diffraction studies carried out at pressures up to 50 GPa [5] and at a temperature reduced to 200 K to overcome the undesirable reaction of lithium with the diamond anvils under pressure have revealed a sequence of phase transitions. According to these measurements, near 39 GPa lithium transforms from high-pressure face-centered-cubic (f.c.c.) phase through an intermediate rhombohedral phase to a cubic body-centered unit cell with 16 atoms (Pearson symbol cI16). The total energy calculations [5] performed by means of the linear muffin-tin orbital method predicted that this phase, observed in elements for the first time, is stable to a pressure of 165 GPa. In our previous work [6], we reported direct measurements of electrical resistivity ρ of lithium compressed by the dynamic methods to 60 GPa, which revealed its anomalous increase by more than an order of magnitude. In this paper, we report new results obtained for lithium quasi-isentropically compressed in multistep shock experiments up to a pressure of 210 GPa and a density of 2.3 g/cm^3. This significantly extends the region of densities studied in previous investigations [3–6].

High pressures and densities in a substance can be generated by isothermal isentropic or dynamic (shock wave) compression techniques. The maximum pressure achieved in static compression experiments is limited by the strength in the diamond anvil, while the pressure limits for the shock-wave method depend only on the driver's power. So, the shock-wave experiments provide for simple and effective means in the investigation of electrical properties and phase transitions in matter at high pressure and temperature. Since the characteristic time of shock-wave experiments is on the order of 10^{-6} s or less, the diffusion processes and chemical interaction between the compressed material and surrounding media play much less destructive roles than in static experiments [3–5], in which the characteristic time is equal to hours or more.

[1] This article was submitted by the authors in English.

The method of multiple shock compression [7] is used in this work to reduce the effects of irreversible heating in the shock-wave front. It allows one to generate the thermodynamic states that can be considered as quasi-isentropical. A lithium sample was placed in an insulator between steel baseplates. The impact of a striker, accelerated to 5 km/s by the detonation products of high explosive, produced an intense shock wave initiating the compression process. Due to the higher dynamic impedance of steel, the shock wave in lithium was progressively reflected from the baseplate reshocking the sample. The sequence of reverberating shocks between baseplates resulted in some final state with higher pressure and lower temperature, in comparison with the case of single shock [7]. Note that the partition of a single shock into successive small shocks substantially decreased the final temperature and increased the final density, making the process more "isentropic." Such a specially designed process of multistep shock compression can be treated as quasi-isentropic. For example, the estimated temperature of a lithium compressed multistep to 100 GPa between stainless steel anvils is ~10 times lower than that which would be achieved by a single shock with the same pressure.

The multiple shock compression of lithium to megabar pressures was performed by special high explosive generators (see Fig. 1 illustrating the experimental setup for the regime of multistep shock compression). The impact of a plane steel projectile initiated a sequence of shock waves in the baseplate–insulator–lithium–insulator–baseplate system. The stainless steel impactor of 3–4 mm thickness was accelerated to 5 km/s by the detonation products of high explosives. The impactor struck the stainless steel baseplate (2–4-mm thick) to initiate a shock wave. Lithium foil (0.07–0.15-mm thick) was placed between polyethylene or teflon insulating plates (0.8–1.0 mm).

The shock in the sample then reverberated back and forth between the base plate and the reflector through insulating plates and the lithium specimen until pressure reached a value equal to the pressure incident initially from the steel. The pulsed generator produced square pulses of magnitude 8.5 A in low-resistance loads. Electric signals from lithium and piezoresistive manganin gauge were recorded with a Tektronix TDS744A digital oscilloscope in the frequency range 0–1 GHz with a 2 ns sampling time. Pressure was measured by a four-point manganin gauge made from 35-μm thick manganin foil and electrodeposited with 5-μm copper layer, excepting its bridge. The use of a four-point scheme excluded any influence due to the resistance of contacts and input leads. The cell was designed in such a way that the lithium specimen and the bridge of the pressure gauge were in the region free from edge effects induced by hydrodynamic disturbances. The cell was assembled in an argon dry box. All gaps were filled with a vacuum lubricant. The pressure range to 100 GPa was investigated at liquid nitrogen (77 K) and room (293 K) initial temperatures. In the

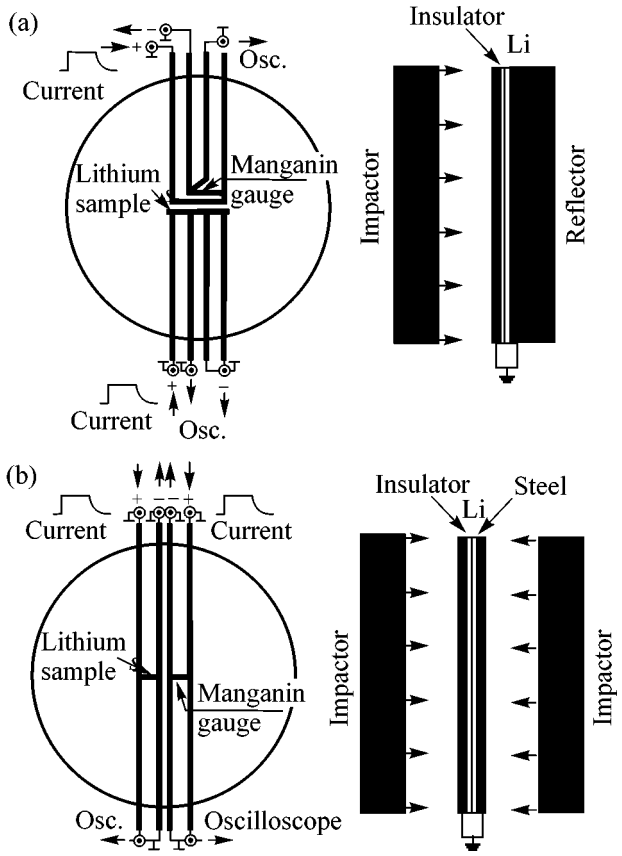

Fig. 1. Experimental setup. (a) Traditional scheme and (b) symmetrical scheme.

second series of measurements, the symmetrical ("front-collision") scheme of compression was used with two high-velocity impactors striking baseplates synchronically on opposite sides. This made it possible to achieve much higher pressures, up to 210 GPa.

The time-resolved characteristics in the experiments were pressure, measured by the manganin gauge, and voltage (and, therefore, resistance), measured with the use of four-point contact probes. The average errors for pressure and resistance were on the order of 5%. 1D numerical modeling was performed to obtain density d and temperature T of lithium under conditions of dynamic experiment. It was carried out using the semiempirical multiphase equation of state [8] (EOS). The EOS model was modified to the full Debye model of crystal [9], to adequately account for the low-temperature states; the obtained EOS of lithium describes the thermodynamic properties of solid, liquid, and plasma states, as well as high-pressure melting, evaporation, and ionization. We used the resistance data, direct measurements of pressure to 100 GPa, and the results of computer simulation to obtain d, ρ and T, while at higher pressures, which were beyond the region of applicability of the manganin gauge, these values were obtained by computer simulation. A

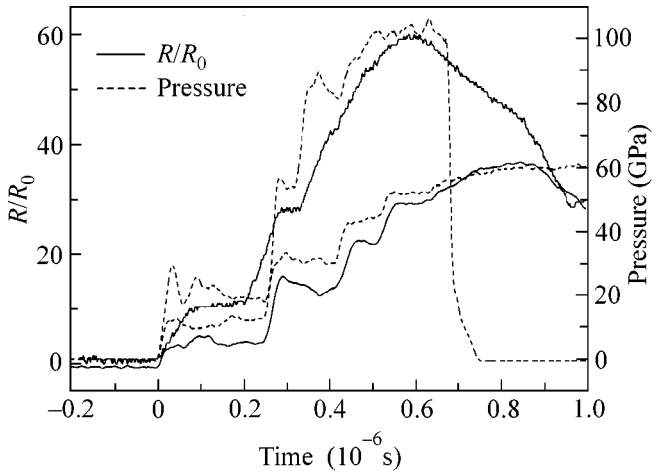

Fig. 2. Relative resistance (left axis) and pressure (right axis) profiles as functions of time in the multishock-compression experiments.

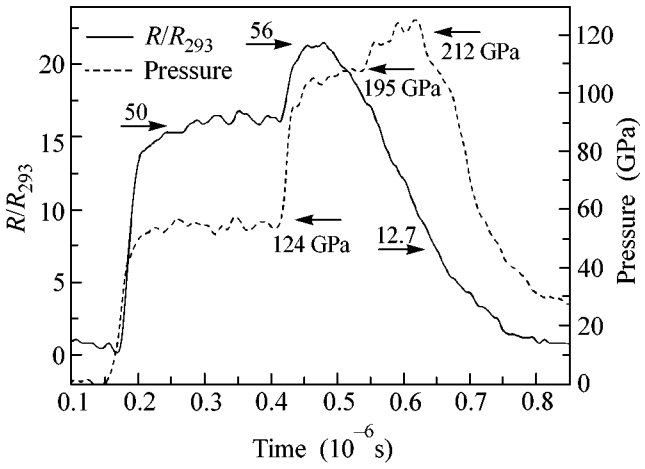

Fig. 3. Relative resistance (left axis) and pressure (right axis) profiles as functions of time in the 212-GPa experiment. Numbers near arrows correspond to the corrected values (see text).

change in the thickness of lithium samples under pressure, resulting in corresponding correction of the resistivity ratio ρ/rho_0 (where ρ_0 is the resistivity at ambient conditions), was also taken into account in analyzing the experimental data. The estimated errors of pressure, density, resistivity, and temperature were about 5%.

In agreement with the general theory of solid state [1], the lithium resistivity at moderate dynamic pressures $P < 10$ GPa slightly increases as pressure and temperature grow. The anomalous region occurs at a dynamic pressure of 40 GPa and higher at normal and low (77 K) initial temperatures. Two experimental resistivity histories of lithium and the corresponding pressure profiles obtained by the manganin gauge are plotted in Fig. 2. Analysis shows that 4–5 steps of sample-resistance and associated pressure steps can be resolved in the experimental recordings. Typically, in other experiments we also could resolve 4–5 individual pressure steps and measure lithium resistivity for each of them. It is evident that pressure grows in steps corresponding to the reflections of the shock wave from steel baseplates. It is important that the resistivity of lithium grows synchronously with pressure in both experiments. Finally, lithium resistivity decreases when the compressed sample starts to expand in the release wave.

The front-collision experiments with two impactors (Fig. 1b) allows one to achieve very high pressure. The maximum pressure in the lithium sample placed between the polyethylene and teflon plates was 160 and 212 GPa, respectively. These experiments were carried out at ambient conditions. The original resistance recordings $R(t)/R_0$ and the corresponding pressure profile from the manganin gauge, obtained in the 212-GPa experiment, are plotted in Fig. 3. Teflon becomes a conductor at such a high pressure, which results in the appearance of an additional load in the experimental circuit. It influences the resistivity of both manganin gauge and lithium sample. The known pressure dependence of manganin resistance allows one to account for the influence of surrounding media on the resistances of the gauge and the sample. The corrected resistance of the lithium sample and the pressure obtained by computer simulation are also plotted in Fig. 3. The experimental recordings demonstrate that the lithium resistance grows as pressure increases to 195 GPa, and then it decreases when pressure reaches its maximum value of 212 GPa. An analogous result was obtained in the 160-GPa multistep-compression experiment. As is seen from Figs. 2 and 3, lithium demonstrates anomalous behavior under high compression. Its resistance changes weakly at pressures lower than 40 GPa, rises anomalously by several orders in the pressure range 40–120 GPa, and becomes again metallic at 160–190 GPa.

The summary of data obtained is given in Fig. 4 in the form of lithium resistivity ρ/ρ_{293} as a function of density. As one can see, the resistivity increases monotonically with density for all experiments corresponding to a maximum pressure of 100 GPa at initial temperatures of 77 K and 293 K. The data obtained at higher pressures (160-GPa and 212-GPa experiments) also agree with these measurements in the investigated density range up to 1.75 g/cm^3. At higher densities on the order of 2.0–2.3 g/cm^3, the specific resistivity decreases dramatically. Lithium melts under conditions of dynamic experiment in the first or second shock waves in the pressure region <7.3 GPa and temperature <530 K, depending on the intensity of the incident shock wave. The final states of dynamically compressed lithium, according to the results of 1D numerical modeling with real EOS, correspond to the liquid state at temperatures from 955 to 2833 K. The esti-

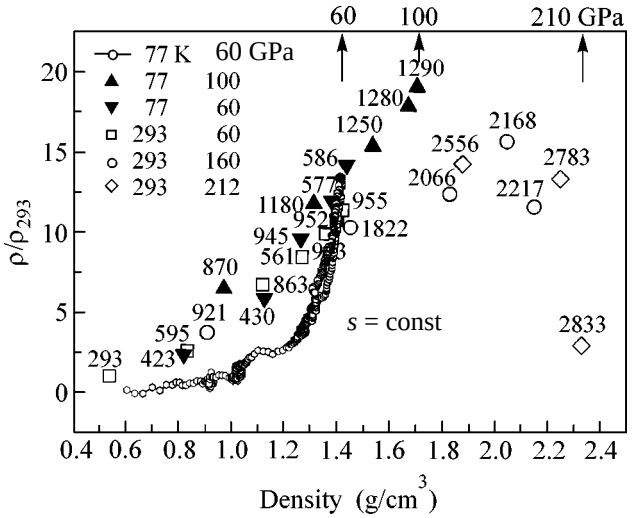

Fig. 4. Resistivity of lithium as a function of density in the multishock-compression experiment. The legend of points includes the initial temperature and the maximum pressure, and numbers near the points show the calculated temperature.

mated thermal component of lithium resistivity ρ/ρ_{293} is on the order of 20–25% of the total value at the maximum density. So, the main reason for the change in lithium resistivity is a decrease in the interatomic distances. Apparently, the anomalous region occurring at 40 GPa and 1.1–1.2 g/cm^3 corresponds to the f.c.c.–cI 16 transition, in accordance with recent results [5]. The high-pressure phase with low conductivity can be either cI 16 or oC 8 (Cmca "paired-atom{predicted by Neaton and Ashcroft [2]) phase. One should note that the dependence of resistivity on density is similar in both solid (quasi-isentropic s = const compression data from previous work [6] are given in Fig. 4) and liquid states. Another interesting and unusual fact is that, under conditions of dynamic experiments, liquid lithium is a poor conductor up to 160 GPa (for example, crystal germanium and silica are typical semiconductors, whereas these materials have good conductivity in liquid state). It seems that compressed liquid lithium has an ordered structure which is broken at 160 GPa, and lithium again becomes a "good" metal (Fig. 4).

Thus, the electrical conductivity of lithium at megabar dynamic pressure demonstrates its anomalous behavior. It changes from typical metallic values to semiconductor ones and then back to metallic. The analysis of experimental data proves that lithium, the first metal in the periodic system of elements having one valence electron, cannot be considered as a "simple" metal at high pressure. We plan to continue the experimental investigation of these exotic effects by performing similar experiments at lower temperatures and high pressures, and also by exploring other alkali metals. First experiments carried out for sodium proved the existence of this effect.

We thank N.W. Ashcroft and E.G. Maksimov for fruitful discussions and for kindly providing lithium samples (NWA).

REFERENCES

1. N. W. Ashcroft and N. D. Mermin, *Solid State Physics* (Holt, Rinehart and Winston, New York, 1976).
2. J. B. Neaton and N. W. Ashcroft, Nature **400**, 141 (1999).
3. V. V. Struzhkin, A. F. Goncharov, R. J. Hemley, *et al.*, in *Science and Technology of High Pressure: Proceedings of International Conference on High Pressure Science and Technology (AIRAPT-17), Honolulu, 1999*, p. 76.
4. Y. Mori and A. L. Ruoff, in *Science and Technology of High Pressure: Proceedings of International Conference on High Pressure Science and Technology (AIRAPT-17), Honolulu, 1999*, p. 75.
5. M. Hanfland, K. Syassen, N. E. Christensen, and D. L. Novikov, Nature **408**, 174 (2000).
6. V. E. Fortov, V. V. Yakushev, V. I. Postnov, *et al.*, Pis'ma Zh. Éksp. Teor. Fiz. **70**, 620 (1999) [JETP Lett. **70**, 628 (1999)].
7. V. N. Postnov, V. V. Yakushev, S. S. Nabatov, *et al.*, Fiz. Goreniya Vzryva **5**, 160 (1983).
8. A. V. Bushman, G. I. Kanel, A. L. Ni, and V. E. Fortov, *Thermophysics and Dynamics of Intense Pulse Loadings* (Taylor and Fransis, London, 1993).
9. L. D. Landau and E. M. Lifshitz, *Course of Theoretical Physics*, Vol. 5: *Statistical Physics* (Nauka, Moscow, 1995; Pergamon, Oxford, 1976).

JETP Letters, Vol. 74, No. 8, 2001, pp. 422–424. Translated from Pis'ma v Zhurnal Éksperimental'noĭ i Teoreticheskoĭ Fiziki, Vol. 74, No. 8, 2001, pp. 462–465.

Magnetic Properties of Crystals of the Molecular Complex between Fullerene C60 and an Organic Donor 9,9'-*trans*-Bis(telluraxanthenyl)

V. V. Kveder[1],* É. A. Shteinman[1], R. N. Lyubovskaya[2], S. A. Omel'chenko[3], and Yu. A. Osip'yan[1]**

[1] *Institute of Solid-State Physics, Russian Academy of Sciences, Chernogolovka, Moscow region, 142432 Russia*

**e-mail: kveder@issp.ac.ru*

***e-mail: shteinman@issp.ac.ru*

[2] *Institute of Problems of Chemical Physics, Russian Academy of Sciences, Chernogolovka, Moscow region, 142432 Russia*

[3] *Dnepropetrovsk University, Dnepropetrovsk, 320625 Ukraine*

Received September 14, 2001

The EPR and static magnetic susceptibility of the crystalline molecular complex between fullerene C60 and an organic donor 9,9'-*trans*-bis(telluraxanthenyl) (BTX) have been measured as functions of temperature. At temperatures T above 130 K, the samples exhibit anomalously high magnetic susceptibility exceeding the values calculated under the assumption that each molecule bears one paramagnetic spin 1/2. A very intense magnetic resonance signal is also observed in the samples in the region of high g factors ($g > 4.5$). This allows the suggestion that the samples under study possess ferromagnetism (or superparamagnetism). The EPR signal and magnetic susceptibility sharply decay almost to zero as the temperature decreases below 100–120 K. It is supposed that electron transfer from donor molecules BTX to C60 molecules takes place at temperatures above 110 K. This electron transfer generates electron spins in the system, whereas the anomalously high magnetism is due to ferromagnetic correlations in the system of these spins. © *2001 MAIK "Nauka/Interperiodica".*

PACS numbers: 76.30.-V; 75.30.Cr; 75.50.-y

The discovery of "soft" ferromagnetism at temperatures below 17 K in the crystalline complex of fullerene C60 with tetrakis(dimethylamino)ethylene (TDAE), one of the strongest organic donors, aroused very strong interest in such complexes [1–4]. Note that ferromagnetism is commonly exhibited by crystals containing ions with unfilled 3*d* or 4*f* shells (Fe, Ni, and so forth), and ferromagnetism in the absence of such ions is a very rare phenomenon.

In C60–TDAE crystals, the TDAE donor level lies higher than the LUMOs of C60 molecules, and electrons transfer from TDAE to C60 molecules. This leads to the appearance of unpaired electron spins and, correspondingly, to paramagnetism. However, the mechanisms of exchange interaction leading to the ferromagnetism of these crystals at $T < 17$ K have not been fully understood so far. It is interesting to note that no deviation from the paramagnetic Curie law is observed in the C70–TDAE complex, in which electron transfer from TDAE to C70 also occurs, giving rise to paramagnetic spins.

The discovery of ferromagnetism in C60–TDAE stimulated works on the synthesis and study of C60 complexes with other organic donors. A great number of such complexes were synthesized (see, for example, [5–10]). In some of these complexes, the donor level lies below the conduction band, which is formed by LUMOs of C60 molecules, and these complexes exhibit no ferromagnetism. In some complexes, the opposite situation occurs, and electron transfer from donors to C60 takes place, which gives rise to paramagnetism and an intense EPR signal with the g factor close to 2 (as well as in C60–TDAE). However, no evidence of ferromagnetic correlations was found in these complexes.

In this work, we report the discovery of unusual magnetic properties in a crystalline molecular complex of C60 and an organic donor 9,9'-*trans*-bis(telluraxanthenyl) (BTX). The crystal structure of C60–BTX studied in [11] is characterized by the P-1 ($Z = 1$) space group and the occurrence of chains of C60 molecules along the "a" direction, where the parameter $a = 1.03$ nm somewhat exceeds the distance 1.002 nm between the centers of the C60 molecules in the C60 crystal. At low temperatures ($T < 20$ K), the C60–BTX crystals exhibit intense photoluminescence [11] in the region 1.1−1.5 eV associated with excited states of C60 molecules. The photoluminescence spectrum (PL) of the complex is shifted by approximately 0.16 eV toward

low energies as compared with the PL of C60 crystals. The photoluminescence decay time in C60–BTX crystals equals 1 ms [12], which exceeds the lifetime of singlet excitons in C60 crystals by several orders of magnitude. The occurrence of intense PL of molecules in C60 complexes commonly points to the absence of a charge on C60. As distinct from C60 crystals, PL in C60–BTX decays rapidly as the temperature increases, and it becomes hardly evident at $T > 60$ K.

Samples and experimental techniques. C60–BTX samples were synthesized by slow (12 days) evaporation of an equimolar solution of C60 and BTX in CS_2 in an argon atmosphere. The synthesis products were small (about 0.1–0.2 mm in size) black-colored crystals. The samples after the synthesis were stored in air without special precautions. The EPR absorption spectra $d\chi''/dH$ were measured at a frequency of 9560 MHz using a low-frequency (127 Hz) modulation of the magnetic field. The sensitivity was calibrated by a paramagnetic standard $CuSO_4 \cdot 5H_2O$. Magnetic susceptibility in low fields was measured from a change in the emf induced in the receiving coil by the external low-frequency magnetic field with a frequency of 830 Hz on introducing the sample into the coil. The system was calibrated by measuring a sample of $CuSO_4 \cdot 5H_2O$ of the same volume.

Results and discussion. EPR spectra observed in C60–BTX powder at various temperatures are displayed in Fig. 1. For convenience of comparison, the amplitude of the EPR signal was normalized to the EPR line of Cu^{2+} ions in the paramagnetic standard (a narrow line on the right-hand side with $g = 2.17$). Two important features engage our attention. First, as distinct from the other charge-transfer complexes of C60 (for example, C60–TDAE), in which an intense signal is observed in the region $g \approx 2$, C60–BTX exhibits a very strong EPR signal in the region of anomalously high g factors, $g > 4.5$. Second, the EPR signal, which only slightly varies at $T > 130$ K, decays suddenly and rapidly almost to zero as the temperature decreases from 120 to 100 K. Such features have been observed in none of the C60 complexes studied previously.

Unfortunately, an analysis of the EPR line shape cannot give much information, because the measurements were performed on powdered samples, and the large width of the EPR spectrum is evidently due to the anisotropy of the g factor. By virtue of the absence of sufficiently large single crystals, we have not managed to investigate the line shape and anisotropy so far.

Curve *1* in Fig. 2 shows the temperature dependence of the magnetic susceptibility of a sample calculated from the intensity of EPR spectra in the range 0.5–3 kOe by integrating them over the magnetic field. Curve *2* in Fig. 2 shows the temperature dependence of the static magnetic susceptibility of a sample in a field of 0–3 Oe measured by the induction method. For comparison, curve *3* in Fig. 2 shows the magnetic susceptibility of the paramagnetic standard ($CuSO_4 \cdot 5H_2O$ sample). Note that the bulk concentration of paramagnetic copper ions ($g \approx 2$, $S \approx 1/2$) in the reference standard sample is approximately 5 times higher than the concentration of C60 molecules in a C60–BTX sample; however, the magnetic susceptibility of a C60–BTX sample at $T > 120$ K is 4–5 times higher than the magnetic susceptibility of the standard.

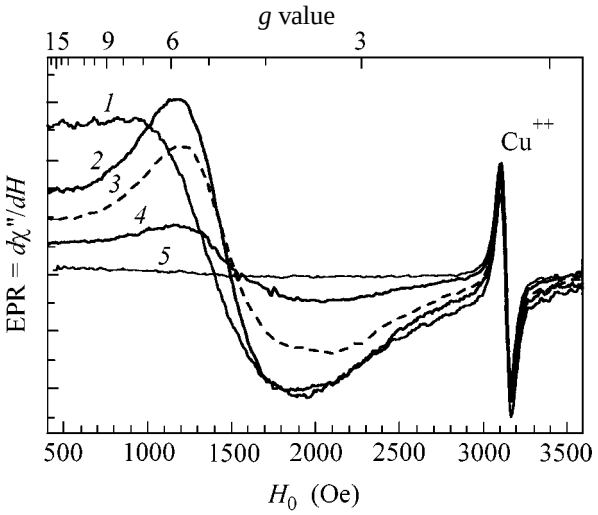

Fig. 1. EPR spectra of C60–BTX powder at various temperatures: (*1*) $T = 189$ K, (*2*) $T = 133$ K, (*3*) $T = 115$ K, (*4*) $T = 111$ K, and (*5*) $T = 90$ K. The amplitudes of EPR are normalized to the EPR of Cu^{2+} ions in a paramagnetic standard.

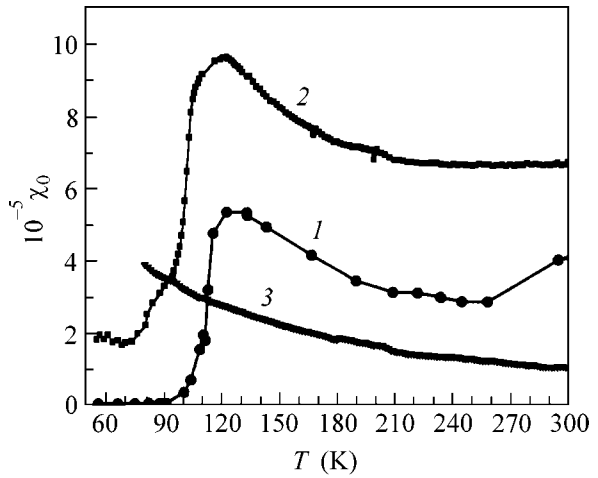

Fig. 2. Temperature dependence of the magnetic susceptibility of a C60–BTX sample: (*1*) calculated from the integral intensity of EPR spectra in the range 0.5–3 kOe, (*2*) measured by the induction method in a field of 0–3 Oe, and (*3*) measured for $CuSO_4 \cdot 5H_2O$.

Thus, we found the following new and unusual facts:

(1) the anomalously high magnetic susceptibility of C60–BTX crystals at temperatures higher than 120 K and the anomalously high g factor of the EPR signal in these samples;

(2) a sharp drop of the magnetic susceptibility and the disappearance of the EPR signal as the temperature T decreases below 110 K.

There are two possible reasons for the sharp drop of the magnetic susceptibility at $T < 110$ K: switching on of antiferromagnetic interaction in the system of spins or a decrease in the number of spins. In our view, a decrease in the number of spins is a simpler and more credible explanation. Assume that the donor level of BTX at low temperatures lies somewhat lower than the bottom of the conduction band, which is formed of the LUMOs of C60 molecules. Then, the concentrations of free electrons on C60 and of paramagnetic holes on BTX molecules at low temperatures are small, and both the magnetic susceptibility and the EPR signal are virtually absent. It may be supposed that, as the temperature increases, the conduction band edge shifts down in energy with respect to the donor level of BTX. At some instance, the donor level of BTX can cross the conduction band edge, which will lead to the appearance of free electrons in the conduction band (on C60) and unpaired paramagnetic spins (holes) on BTX molecules. The occurrence of paramagnetism at elevated temperatures can be explained within the framework of this model. However, in order to explain the anomalously high g factor and anomalously high magnetic susceptibility, it is necessary to suggest the occurrence of ferromagnetic interaction between electron spins.

It should be noted that measurements performed on C60–BTX samples of different lots give qualitatively similar results, though the absolute values of the EPR signal and the magnetic susceptibility in different samples strongly differ (several times). This suggests that the samples are not uniform in magnetic properties and that only part of the crystals possess ferromagnetic properties. A similar wide scatter of magnetic properties is also observed in the case of C60–TDAE (see [1–4]). The reasons for the wide scatter of the magnetic properties of C60–TDAE crystals were recently studied in [13]. According to [13], the mutual orientation of C60 molecules in the crystal is a very important parameter determining the occurrence of ferromagnetism. The orientational ordering of C60 molecules strongly depends on the synthesis conditions and thermal prehistory of the samples, which explains the strong difference in the observed magnetic properties of C60–TDAE crystals. Thus, the C60–TDAE samples synthesized at a low temperature (8°C) exhibit no traces of ferromagnetism down to 2 K, but they exhibit a ferromagnetic transition at 16 K after annealing for 6 h at 70°C. It is possible that the scatter of magnetic properties in samples of different lots observed in our experiments is due to similar reasons.

The elucidation of the nature of the unusual properties of C60–BTX crystals needs further investigation. In particular, it will be interesting to investigate the anisotropy of the magnetic susceptibility and the g factor, the dependence of the magnetic moment on the magnetic field in high fields, and the temperature dependence of optical absorption spectra. In order to perform these investigations, it is desirable to have sufficiently large single crystals, which, unfortunately, have not been obtained so far.

REFERENCES

1. P.-M. Allemand, K. C. Khemani, A. Koch, *et al.*, Science **253**, 301 (1991).
2. K. Tanaka, A. A. Zakhidov, K. Yoshizawa, *et al.*, Phys. Rev. B **47**, 7554 (1993).
3. B. Gotschy, Phys. Rev. B **52**, 7378 (1995).
4. D. Arcon, P. Cevc, A. Omerzu, and R. Blinc, Phys. Rev. Lett. **80**, 1529 (1998).
5. A. Izuoka, T. Tashikawa, T. Sugawara, *et al.*, J. Chem. Soc., Chem. Commun., 1472 (1992).
6. A. Izuoka, T. Tachikawa, T. Sugawara, *et al.*, Chem. Lett., 1049 (1992).
7. P. Wang, W.-J. Lee, I. Shcherbakova, *et al.*, Synth. Met. **64**, 319 (1994).
8. A. Penicaud, A. Perez-Benitez, V. R. Gleason, *et al.*, J. Am. Chem. Soc. **115**, 10392 (1993).
9. U. Bilow and M. Jansen, J. Chem. Soc., Chem. Commun., 403 (1994).
10. W. C. Wan, X. Liu, G. M. Sweeney, and W. E. Broderick, J. Am. Chem. Soc. **117**, 9580 (1995).
11. V. V. Kveder, É. A. Steinman, B. Zh. Narymbetov, *et al.*, Chem. Phys. **216**, 407 (1997).
12. É. A. Steinman, V. V. Kveder, D. V. Konarev, *et al.*, Chem. Phys. Lett. **319**, 1 (2000).
13. B. Narymbetov, A. Omerzu, V. Kabanov, *et al.*, Nature **407**, 883 (2000).

Translated by A. Bagatur'yants

JETP Letters, Vol. 74, No. 8, 2001, pp. 425–430. Translated from Pis'ma v Zhurnal Éksperimental'noĭ i Teoreticheskoĭ Fiziki, Vol. 74, No. 8, 2001, pp. 466–471.

On the Theory of Giant Magnetoresistance (Longitudinal Current)

V. Ya. Kravchenko

Institute of Solid State Physics, Russian Academy of Sciences, Chernogolovka, Moscow region, 142432 Russia

Received September 18, 2001

The problem of conductivity of a multilayer sample (alternating magnetic and nonmagnetic metal layers) with a current parallel to its surfaces is solved using a set of kinetic equations. Conditions at which the conductivity variations associated with changes in the type of magnetization alignment in adjacent layers reach the values on the order of initial conductivity are considered. Parameters governing the giant magnetoresistance effect and the relations between them are determined. © *2001 MAIK "Nauka/Interperiodica".*

PACS numbers: 75.70.Pa; 73.40.-c

1. The giant magnetoresistance (GMR) effect is observed in layered systems consisting of alternating ferromagnetic (*m*) and nonmagnetic (*n*) metal layers. Sequential *m* layers change from the initial antiparallel (AP) alignment of their magnetizations to the parallel (P) one under the effect of a relatively weak magnetic field (much weaker than the fields producing noticeable magnetoresistance in massive samples of the same metals). This is accompanied by a considerable change in the resistance of the multilayer structure (relative changes reach several tens of percent). The first experimental studies of the GMR are described in [1, 2], and the reviews can be found in [3–6]. In the first experiments, a decrease in the resistance, i.e., a negative effect (GNMR), was observed. Later, a change from the AP orientation to the P one was found to be accompanied by an increase in the resistance, i.e., by a positive (or inverse) effect. The possible mechanisms underlying the GMR effect were discussed in many theoretical publications. In some papers, the analysis was performed starting from the first principles (according to the authors' terminology) [7–11]: the electronic structure was modeled for specific variants of monatomic plane packing in the layers, and, then, specific electron modes localized near the surfaces were determined and their contributions to the conductivity changes were found. These studies were based on the models and numerical estimates and hardly revealed the general physical pattern of the effect. Another approach uses a semiclassical description with allowance for the spectral characteristics of electrons in the "parent" *n* and *m* metals, and the conductivity of the system is calculated using either a Greens' function formalism [12–15] or kinetic equations [16–20] (in the semiclassical approximation, these methods are equivalent). However, the theoretical analysis performed in the cited publications is, in our opinion, somewhat incomplete and, in certain cases, even incorrect. For example, questions arise as to the boundary conditions, which involve not only the usual Fuchs parameters [21, 22], but also the transmission coefficients (for transmissions between the *m* and *n* layers). In some publications, these coefficients were assumed to be coincident over the whole domain of momentum variations [17, 20], whereas in other publications, the diffuse components were assumed to be equal and the specular components were treated using simplified optical analogues [18, 23]. As a result, important contributions to the spin dependence of transmission parameters were omitted. In addition, the relative contributions of the *n* and *m* electrons to the alignment-dependent conductivity were not estimated. No answer was given to the questions of what should be the ratio between the specular and diffuse scattering components at the layer boundaries for the giant effect to be realized and what are the factors that determine the sign of this effect.

This study is devoted to the theoretical analysis of the problem of longitudinal current in a multilayer system (the so-called CIP geometry) on the basis of a set of kinetic equations. The boundary conditions for the distribution functions at the interlayer boundaries are formulated using the generalized Fuchs parameters. The dependence of the conductivity variation on the parameters of the *n*- and *m*-electron energy spectra is investigated, and the factors that govern the magnitude and the sign of the GMR effect are determined.

2. Equations of the problem. For the distribution function of electrons with momentum $\mathbf{p}$, energy $\varepsilon_{\mathbf{p}}^{s}$, and spin projection s ($s = \pm 1$ is the sign of spin projection on the quantization axis) in an arbitrary layer $i = (n_j, m_j)$, we use the expression

$$f_i^s = f_{0i}^s + \frac{\partial f_{0i}^s}{\partial \varepsilon_{ip}^s}\chi_i^s, \qquad (1)$$

0021-3640/01/7408-0425$21.00

where $f^s_{0i} = f_0(\varepsilon^s_{ip} - \mu)$ is the equilibrium Fermi function. We limit our consideration to a simple parabolic spectrum of the carriers:

$$\begin{aligned}\varepsilon^s_{n_jp} &= \varepsilon_{np} = p^2/2m_n + \varepsilon_n,\\ \varepsilon^s_{m_jp} &= p^2/2m_m + \varepsilon_m - \Omega_j s.\end{aligned} \tag{2}$$

In Eqs. (2), the reference points of the *n* and *m* spectra are specified; the presence of magnetization is expressed in the form of Zeeman spin energy $\Omega_j s$; in the case of P packing, all Ω_j are identical, and, in the case of AP packing, they change sign each time as the index *j* changes by unity. In the equation for the nonequilibrium component $\chi^s_i(\mathbf{p})$, we express the collision integral through the relaxation times:

$$v_z\frac{\partial\chi^s_i}{\partial z} + \frac{\chi^s_i}{\tau_{si}} = -ev_xE_x, \tag{3}$$

where E_x is the electric field strength, $1/\tau_{si}$ is the frequency of scattering from the state *s*, and the *z* axis is directed normally to the layers. Let us introduce the notation for the Fermi momenta:

$$\begin{aligned}p_{si} &= p_i\sqrt{\Gamma_{si}},\quad p_i = \sqrt{2m_i(\mu-\varepsilon_i)},\\ \Gamma_{si} &= 1 + s\frac{\Omega_i}{\mu-\varepsilon_m}.\end{aligned} \tag{4}$$

The parameter Γ_{sj} characterizes the differences in the energy shifts of the *s* groups; these shifts occur only for *m* electrons (for *n* electrons, $\Gamma_{sn} = 1$). Using Eqs. (4), we write the following expressions for the momenta from Eqs. (2) at $\varepsilon^s_i = \mu$ and for the partial densities of states:

$$p^2 = p_z^2 + p_\parallel^2 = p_i^2\Gamma_{si},\quad \nu^s_{iF} = \frac{p_im_i}{2\pi^2\hbar^3}\sqrt{\Gamma_{si}}, \tag{5}$$

where $\mathbf{p}_\parallel$ is the electron-momentum component parallel to the layer surfaces.

We limit our consideration to the case of a dominant elastic scattering and to the case when the spin-dependent components of the potentials can be neglected. Then, we can ignore the contribution of the transitions with spin projection reversal $s \longrightarrow -s$. Taking into account that the scattering frequency is proportional to the density of final states at the chemical potential level ν^s_i, it is convenient to recast the relaxation times according to the formula

$$1/\tau_{si} = \sqrt{\Gamma_{si}}/\tau_i, \tag{6}$$

where the "nominal" times τ_i do not depend on *s*. For definiteness, we assume that the outer surfaces of the sample are *n* layers. We also assume that the layer thickness is the same for the same type of layers; i.e., we have two thicknesses d_n and d_m, so that the total thickness of the sample is $D = D_m + D_n$, where $D_m = Kd_m$ and $D_n = (K+1)d_n$. The boundary conditions at the surfaces between the layers *j* and *j*' have the form

$$\begin{aligned}\chi^{s>}_{j'l}(r) &= [t^{jsp}_{cj's}\chi^{s>}_{jr}(\tilde p_t(s)) + r^{j'sp}_{cs}\chi^{s<}_{j'l}(\tilde p_r(s))],\\ \tilde{\mathbf{p}}_\mathbf{t}(s) &= (\mathbf{p}_\parallel, \sqrt{p^2_{js} - p^2_\parallel}),\\ \tilde{\mathbf{p}}_\mathbf{r}(s) &= (\mathbf{p}_\parallel, \sqrt{p^2_{j's} - p^2_\parallel}).\end{aligned} \tag{7}$$

Here, t_c and r_c are the coefficients of a specular transmission through the boundaries and reflection from them, respectively. The subscripts $r(l)$ correspond to the right (left) boundary of the *j*th or *j*'th layer; the subscripts marking the quantities $\tilde{\mathbf{p}}$ indicate the initial momenta for the transmission and reflection, respectively; and the signs > (<) correspond to the positive (negative) values of the velocity v_z. The conditions for $\chi^{s<}_{jrp}$ (on the other side of the boundary $z = z_{jj'}$) have a similar form. The parameters $\hat t_c$ depend on the momentum:

$$t^{jsp}_{cj's} = t^{j'sp}_{cjs} = t^{js}_{cj's}\Theta[\min(p_{js}, p_{j's}) - p_\parallel], \tag{8}$$

where Θ is Heaviside unit step function determining the region of the coincidence of longitudinal momenta, and the coefficients $t^{js}_{cj's} = t^{j's}_{cjs}$ are assumed to be constant. The normalization conditions, which relate the specular and diffuse parameters for the transitions from the (*jsp*) states to all possible states (with the same value of *s*), are as follows:

$$t^{jsp}_{cj's} + r^{jsp}_{cs} + \zeta^j_{j's} = 1. \tag{9}$$

Here, we introduced the total diffusivity parameter $\zeta^{js}_{j's}$, which is assumed below to be independent of *p*. The details of the derivation of the boundary conditions and relations between the parameters can be found in [24].

We represent the solution to Eq. (3) within the layer m_j in the form

$$\begin{aligned}\chi^{s>}_{m_j} &= -eE_xv_x\tau_{sm_j}\left[1 - (1-\alpha^s_{m_j})\exp\left(-\frac{z - z^l_{m_j}}{v_z\tau_{sm_j}}\right)\right],\\ &\qquad v_z \ge 0,\\ \chi^{s<}_{m_j} &= -eE_xv_x\tau_{sm_j}\left[1 - (1-\beta^s_{m_j})\exp\left(-\frac{z - z^r_{m_j}}{v_z\tau_{sm_j}}\right)\right],\\ &\qquad v_z \le 0.\end{aligned} \tag{10}$$

Similar expressions can be written for $\chi^s_{n_j}$. To determine the values of parameters $\alpha(\beta)$, through which the effect of the specular component of scattering from the left (right) layer boundary on the electron distribution is

expressed, it is necessary to solve the set of equations following from boundary conditions (7).

Let us assume that all boundaries between n and m layers have the same structure, so that the difference in their scattering properties for n electrons is exclusively determined by different orientations of the magnetizations of the m layers adjacent to the n-layer boundaries. Therefore, the transmission t and reflection r parameters corresponding to different boundaries are related to each other in a certain way. In the case of P orientation, the following evident equalities must be satisfied:

$$\begin{aligned}
&\Gamma_{sm_j} = \Gamma_{sm_{j\pm1}} \equiv \Gamma_s, \quad \kappa_{sj} \equiv \kappa_s,\\
&r_{s(r)}^{sn_jp} = r_{s(l)}^{sn_jp} = r_{s(r,\,l)}^{sn_{j\pm1}p} \equiv r_s^{snp},\\
&t_{sm_j}^{sn_jp} = t_{sm_j}^{sn_{j-1}p} = t_{sm_{j+1}}^{sn_jp} \equiv t_{sm}^{snp},\\
&r_{s(r)}^{sm_jp} = r_{s(l)}^{sm_jp} = r_{s(r,\,l)}^{sm_{j\pm1}p} \equiv r_s^{smp},\\
&t_{sn_{j-1}}^{sm_jp} = t_{sn_j}^{sm_jp} = t_{sn_j}^{sm_{j+1}p} \equiv t_{sn}^{smp}.
\end{aligned} \tag{11}$$

The exceptions are outer surfaces of the n_0th and n_Kth layers, where the equality $t = 0$ must be valid. By virtue of Eqs. (11), the set of equations for α and β is reduced to equivalent pairs of equations for two adjacent layers, with the exception of the equations that involve the parameters of outer surfaces. Were it not for this exception, the following simple relationships would be valid:

$$\alpha_{n_j}^s = \beta_{n_j}^s = A_n^s, \quad \alpha_{m_j}^s = \beta_{m_j}^s = A_m^s. \tag{12}$$

The deviations from these equalities depend on the specific number of a layer, and (as can easily be shown [24]) the greater the total number of layers, the smaller these deviations ($\propto 1/K$). Neglecting the aforementioned corrections, we obtain the following equations for the quantities A:

$$\begin{aligned}
A_n^s - R_s^{sn}(p)A_n^s - T_{sn}^{sm}(p)A_m^s/\kappa_s &= r_{sc}^{snp}\hat{g}_n + t_{snc}^{smp}\hat{g}_m^s/\kappa_s,\\
A_m^s/\kappa_s - R_s^{sm}(p)A_m^s/\kappa_s - T_{sm}^{sn}(p)A_n^s &= r_{sc}^{smp}\hat{g}_m^s/\kappa_s + t_{smc}^{snp}\hat{g}_n.
\end{aligned} \tag{13}$$

$$R_s^{sn_j}(p) = r_{sc}^{sn_jp}(1-\hat{g}_n), \quad R_s^{sm_j}(p) = r_{sc}^{sm_jp}(1-\hat{g}_{m_j}^s),$$

$$T_{sm_j}^{sn_{j'}}(p) = t_{sm_jc}^{sn_{j'}p}(1-\hat{g}_n), \quad T_{sn_j}^{sm_{j'}} = t_{sn_jc}^{sm_{j'}p}(1-\hat{g}_{m_{j'}}^s).$$

Here,

$$\begin{aligned}
\hat{g}_n &= 1 - \exp\left(-\frac{d_n}{\tau_n \hat{V}_{zn}}\right),\\
\hat{g}_{m_j}^s &= 1 - \exp\left(-\frac{d_m}{\tau_{sm_j}\hat{V}_{sm}}\right),\\
\hat{V}_{zn} &= \sqrt{p_n^2 - p_\parallel^2}/m_n, \quad \hat{V}_{zm} = \sqrt{p_{sm}^2 - p_\parallel^2}/m_m,
\end{aligned} \tag{14}$$

$$\kappa_{sj} = \frac{m_m\tau_n}{m_n\tau_{sm_j}} = \frac{M_n}{M_{m_j}^s},$$

and M_n and $M_{m_j}^s$ are the electron mobilities in the n and m layers.

Using similar considerations, it is easy to establish the correspondence between the parameters for the case of AP packing and to determine the relations between the quantities α and β:

$$\begin{aligned}
\alpha_{n_i}^s = \beta_{n_i}^{-s} = \alpha_{n_{i\pm1}}^{-s} = \beta_{n_{i\pm1}}^s = A_{1n}^s,\\
\alpha_{m_i}^s = \beta_{m_i}^s = \alpha_{m_{i\pm1}}^{-s} = \beta_{m_{i\pm1}}^s = A_{1m}^s.
\end{aligned} \tag{15}$$

The equations for A_1 are obtained from Eqs. (13) by replacing A with A_1 in such a way that, in the terms with the coefficients T and R, A_n^s should be replaced by A_{1n}^{-s}, whereas, for other replacements, the spin indices should be retained. The conductivity variation for the AP $\longrightarrow$ P reorientation is determined by the parameters

$$\delta A_n^s = A_n^s - A_{1n}^{-s}, \quad \delta A_m^s = A_m^s - A_{1m}^s, \tag{16}$$

which are obtained from the following equations:

$$\begin{aligned}
\delta A_n^s - R_s^{sn}(p)\delta A_n^s - T_{sn}^{sm}(p)\delta A_m^s/\kappa_s &= A_{1n}^{as},\\
\delta A_m^s/\kappa_s - R_s^{sm}(p)\delta A_m^s/\kappa_s - T_{sm}^{sn}(p)\delta A_n^s &= 0.
\end{aligned} \tag{17}$$

Here,

$$F^{as} = F^s - F^{-s} \quad (F^a = F^+ - F^-). \tag{18}$$

Calculating the current density in the layers and passing to its value averaged over the sample thickness, we obtain the mean conductivity of a multilayer sample σ, which can be represented as the sum of two components:

$$\sigma = \frac{1}{D}\int_0^D dz \sum_s \sigma_i^s(z) = \sigma_{bd} + \sigma_c. \tag{19}$$

The component σ_{bd} corresponds to the conductivity of a multilayer sample in the case of a perfectly diffuse scattering at the surfaces:

$$\sigma_{bd} = \sigma_b - \sigma_d, \tag{20}$$

where σ_b is a combination of the bulk conductivities of the materials:

$$\begin{aligned}
\sigma_b &= \sigma_{bn} + \sigma_{bm}, \quad \sigma_{bn} = \frac{D_n}{D}\sigma_{0n},\\
\sigma_{bm} &= \frac{D_m}{D}\sigma_{0m}, \quad \sigma_{0n,\,m} = \sum_s \sigma_{0n,\,m}^s,
\end{aligned} \tag{21}$$

and σ_d describes the "diffuse" reduction of bulk conductivity:

$$\sigma_d = \sigma_d(n) + \sigma_d(m),$$
$$\sigma_d(n) = \frac{3D_n}{2D}\sum_s \sigma_{0n}^s Y_n(u_n g_n l_n/d_n), \quad (22)$$
$$\sigma_d(m) = \frac{3D_m}{2D}\sum_s \sigma_{0m}^s Y_m(u_m g_m^s l_m/d_m).$$

Here,

$$Y_i(x_i) = \int_0^1 du_i(1-u_i^2)x_i, \quad u_i = p_z/p_{si},$$
$$g_i = 1 - \exp\left(-\frac{d_i}{u_i l_i}\right), \quad l_i = v_i\tau_i, \quad v_i = p_i/m_i, \quad (23)$$
$$\sigma_{om_j}^s = \frac{1}{2}\sigma_{0m}\Gamma_{js}, \quad \sigma_{0n}^s = \frac{1}{2}\sigma_{0n},$$

l represents the mean free paths that are independent of s in the adopted approximation, and σ_{0i} are the bulk conductivities. The sums over s, which are involved in Eqs. (21) and (22), contain only the terms depending on the local properties of a given (nth or mth) layer. This fact indicates the absence of correlations between the layers and, hence, the absence of the effect of magnetic-order changes in the sample on the conductivity component σ_{bd}.

The second component σ_c of mean conductivity given by Eq. (19) is related to the GMR effect. This component is determined by the "specular" transitions at the layer boundaries. The corresponding expression for the case of P configuration has the form

$$\sigma_c^{\mathrm{P}} = \sigma_c^{\mathrm{P}}(m) + \sigma_c^{\mathrm{P}}(n),$$
$$\sigma_c^{\mathrm{P}}(n) = \frac{3}{4}\sigma_{bn}\sum_s Y_n(u_n l_n g_n A_n^s/d_n), \quad (24)$$
$$\sigma_c^{\mathrm{P}}(m) = \frac{3}{4}\sigma_{bm}\sum_s Y_m(u_m l_m g_m^s A_m^s/d_m).$$

A similar expression can be written for σ_c^{AP}. The conductivity variation that is of most interest has the form

$$\delta\sigma_c = \sigma_c^{\mathrm{P}} - \sigma_c^{\mathrm{AP}} = \delta\sigma_c(n) + \delta\sigma_c(m), \quad (25)$$

where the expressions for $\delta\sigma$ differ from Eqs. (24) by the substitution of δA for A in the arguments of the integrals Y_n and Y_m determined by Eqs. (23).

3. Results and discussion. To determine the conditions that are necessary for the giant variations of the conductivity to occur, we first consider the situations in which this effect is impossible. Primarily, it is the case of thick layers with $d_i \gg l_i$, where $i = n, m$. In this case, both the diffuse σ_d and the specular σ_c corrections are negligibly small: the variations of σ due to the surface scattering do not exceed the values $\leq\sigma(l/d)$. The effect of interest is also impossible in the case of thick n layers and thin m layers with $d_m \ll l_m$. In this case, noticeable specular contributions to the conductivity of the m layers are possible (with insignificant variations of the n components), but almost no difference is observed between them for the cases of P and AP packings: according to Eqs. (17), the quantities δA_m^s are proportional to the specular parameters T^n from Eqs. (14), and these parameters are exponentially small when $d_n \gg l_n$.

Thus, a giant effect can be expected in the following cases: (i) only n layers are thin,

$$l_n \gg d_n, \quad l_m \ll d_m; \quad (26)$$

(ii) layers of both types are thin,

$$l_m \gg d_m, \quad l_n \gg d_n; \quad (27)$$

and (iii) the set of surface-scattering parameters necessarily contains specular components.

Results demonstrating the most favorable conditions for the realization of giant conductivity variations are presented below (simple calculations are omitted). Considerable difference in such realizations are associated with different possible variants of the relative values of Fermi momenta p_n and p_{ms}.

Variant 1: $p_{ms} > p_n$. We begin with the situation when the specular component dominates, and the diffuse surface scattering is less significant than the volume scattering (characterized by the functions g from Eqs. (14), which depend on d/l):

$$t_c, r_c \gg d/l \gg \zeta. \quad (28)$$

If conditions (28) are satisfied, the specular components make a dominant contribution to the total conductivity. In the case determined by inequalities (26), all giant variations of σ occur in the n layers:

$$\delta\sigma_c(n) \simeq \frac{\sigma_{bn}\Gamma_a t_c^a}{2\sqrt{\Gamma_+\Gamma_-}\sum_s \kappa_s\left[\sum_s t_c^s - t_c^+ t_c^-\right]}. \quad (29)$$

In the case corresponding to inequalities (27), both types of layers contribute to the conductivity variations:

$$\delta\sigma_c(n) \simeq -\sigma_{bn}\frac{\Gamma_a^2}{10\kappa\sum_s \Gamma_s^{-1/2}\Gamma_+^2\Gamma_-^2 q^2(1+\delta)^2}, \quad (30)$$

$$\delta = d_n l_m/d_m l_n, \quad q_s = q\sqrt{\Gamma_s}, \quad q = p_m/p_n.$$

The contribution made by the m layers to the conductivity variation is sensitive to the parameter q_s given by Eqs. (30). When $q_s \gg 1$, the resulting conductivity variation reduces to that determined by Eq. (30); i.e., in contrast to Eq. (29), it corresponds to the so-called

inverse effect. A different situation takes place for $q_+ \gg 1$ and $q_- \simeq 1$. In this case, a considerable contribution to $\delta\sigma_c$ comes from the m-electron branch with $s = -1$:

$$\delta\sigma_c(m) \simeq \frac{\sigma_{bm}}{4}\frac{\Gamma_a\Gamma_-(1+\kappa_-\delta)}{(1+\delta)^2\kappa\sqrt{\Gamma_+\Gamma_-}\sum_s\Gamma_s^{1/2}}, \quad (31)$$

which can considerably (up to a change of sign) affect the final result.

Now we consider the case where the specular coefficients dominate, but the diffuse surface scattering prevails over the volume scattering:

$$t_c, r_c \gg \zeta \gg \lambda, \quad \lambda = \frac{3d}{4l}\ln\frac{l}{d}. \quad (32)$$

Here, λ is a known dimensional factor [21, 22]. In the case determined by inequalities (26), conditions (32) yield a result coinciding with Eq. (29). If inequalities (27) are valid, conditions (32) lead to a dimensional dependence of conductivities. For the limiting situation $q_s \gg 1$, we obtain

$$\delta\sigma_c \simeq \delta\sigma_c(n) \simeq \sigma_{bn}\lambda_n \times \frac{(\zeta_n^a + \zeta_m^a)^2}{(\zeta_n^+ + \zeta_m^+)(\zeta_n^- + \zeta_m^-)\sum_s(\zeta_n^s + \zeta_m^s)}. \quad (33)$$

Finally, we consider the case where the diffuse surface coefficients also exceed the specular parameters:

$$\zeta \gg t_c, r_c, \lambda. \quad (34)$$

The conductivity variation occurs only if conditions (27) are satisfied, and it is reduced only to $\delta\sigma_c(n)$:

$$\delta\sigma_c(n) \simeq \sigma_{bn}\lambda_n\frac{(\zeta_n^a)^2}{\zeta_n^+\zeta_n^-\sum_s\zeta_n^s}. \quad (35)$$

According to Eq. (9), the difference parameter is $\zeta_n^a = -t_{cm}^{na} - r_c^{na}$, and, therefore, in view of Eq. (33), the scale of the conductivity variations should be smaller than in the previous cases.

For two other possible relations between the Fermi momenta, we consider only the limiting situations, which occur for the limiting asymmetry of the s branches of the m-electron spectrum, when the m-electron states with projection $s = -1$ can be neglected (e.g., the density of states of such carriers at the Fermi level is $\nu_m^- \sim p_{-m} \longrightarrow 0$); in the nonmagnetic layers, electrons with both projections are significant.

Variant 2: $p_{+m} > p_n (> p_{-m})$;

Variant 3: $p_n > p_{+m}$.

Calculations show that, under conditions (26) and (28) or (32), we have

$$\delta\sigma_c(n) \simeq \frac{\sigma_{bn}}{2\kappa_+}\begin{cases}\kappa_+ - 1, & \zeta_n^- \ll d_n/l_n \\ -1, & \zeta_n^- \gg d_n/l_n\end{cases} \quad (36)$$

(for variant 3, only the case of close Fermi momenta $q_+ \simeq 1$ is significant, for which the result coincides with Eq. (36); if $q_+ \ll 1$, the quantity $\delta\sigma_c$ is negligibly small).

If the layers of both types are "thin" (27), condition (28) is valid, and the Fermi momenta p_n and $p_{+m}(q_+ \simeq 1)$ are close to each other, the total value of $\delta\sigma_c$ is positive:

$$\delta\sigma_c \simeq \frac{\sigma_{bn}}{2(1+\delta)(1+2\delta)}\left(1 - \frac{1}{\kappa_+}\right)^2. \quad (37)$$

In the limiting cases $q_+ \gg 1$ (variant 2) and $q_+ \ll 1$ (variant 3), the n and m contributions, respectively, dominate and determine the final result:

$$\text{variant 2:}\ \delta\sigma_c \simeq \delta\sigma_c(n) \simeq \sigma_{bn}\frac{(\kappa_+ - 1)}{\kappa_+(1+\delta)(1+2\delta)},$$
$$\text{variant 3:}\ \delta\sigma_c \simeq \delta\sigma_c(m) \simeq -\sigma_{bm}^+\frac{\delta(\kappa_+ - 1)}{(1+\delta)(1+2\delta)}. \quad (38)$$

If conditions (32) are satisfied, for the same limiting relations between the Fermi momenta, we obtain

$$\delta\sigma_c(n) \simeq \sigma_{bn}\lambda_n\frac{(\zeta_n^a + \zeta_m^+)^2}{\zeta_n^-(\zeta_n^+ + \zeta_m^+)\left(\zeta_m^+ + \sum_s\zeta_n^s\right)}, \quad (39)$$
$$\delta\sigma_c(m) \simeq 0$$

for variant 2, while for variant 3 the conductivity varies for both n electrons [the corresponding expression coincides with Eq. (38)] and m_+ electrons,

$$\delta\sigma_c(m) \simeq \sigma_{bm}^+\lambda_m\frac{\zeta_n^-}{(\zeta_n^+ + \zeta_m^+)\left(\zeta_m^+ + \sum_s\zeta_n^s\right)}. \quad (40)$$

The result obtained for relations (33) coincides with Eq. (34).

The set of expressions presented above for $\delta\sigma_c$ demonstrates a variety of possibilities for obtaining giant variations of conductivity. The following important result should be noted: conductivity variations of both signs are possible; i.e., both direct and inverse GMR effects may occur. The scope of this paper does not include a quantitative comparison with experiments. Such a comparison requires the data on the ratio between l and d and on the surface scattering; it is also necessary to use the actual energy spectra of layered metals (note that a Fe/Cr system can be associated with variant 1 introduced above for the relation between the

Fermi momenta, and a Co/Cu system can be treated using variant 2 or variant 3, depending on whether p_{Cu} is close to one or another Fermi momentum of Co—see, e.g., [25]). Some general consequences of the analysis described above can be compared with the experiments from the viewpoint of qualitative agreement. For example, in some experiments, it was found that special treatment of the interlayer boundary surfaces, which enhanced (reduced) their specular properties, resulted in a considerable increase (decrease) in the magnitude of the GMR [26–28]; the studies of the dependence of the GMR effect on the layer thickness showed that the effect became smaller when the thickness d_m increased [29, 30]; it was also found that the GMR effect increased and then reached saturation with increasing number of m/n pairs of layers [29]. One of the results presented above is the existence of a difference between the values characterizing the GMR effect in a multilayer structure satisfying conditions (26) and a sample of the same composition but with a set of layer thicknesses satisfying conditions (27). The experimental verification of this result, which predicts considerable and even qualitative changes (up to a change of sign), seems to be possible and desirable.

I am grateful to É.I. Rashba for valuable advices.

This work was supported by the Russian Foundation for Basic Research, project no. 01-02-16418.

REFERENCES

1. M. N. Baibich, J. M. Broto, F. Fert, *et al.*, Phys. Rev. Lett. **61**, 2472 (1988).
2. G. Binasch, P. Grunberg, F. Sauerbach, and W. Zinn, Phys. Rev. B **39**, 4828 (1989).
3. P. M. Levy, Solid State Phys. **47**, 367 (1994).
4. M. A. M. Gijs and G. E. W. Bauer, Adv. Phys. **46**, 285 (1997).
5. J.-Ph. Ansermet, J. Phys.: Condens. Matter **10**, 6027 (1998).
6. A. Barthelemy, A. Fert, and F. Petroff, *Handbook of Magnetic Materials*, Ed. by K. H. J. Buschow (Elsevier, Amsterdam, 1999), Vol. 12.
7. P. Zahn, I. Mertig, M. Ritcher, and H. Eschrig, Phys. Rev. Lett. **75**, 2996 (1995).
8. W. H. Butler, X.-G. Zhang, D. M. C. Nickolson, and J. M. MacLaren, Phys. Rev. B **52**, 13399 (1995).
9. M. D. Stiles, J. Appl. Phys. **79**, 5805 (1996).
10. K. Schep, P. J. Kelly, and G. E. Bauer, Phys. Rev. Lett. **74**, 586 (1995); Phys. Rev. B **57**, 8907 (1998).
11. C. Blaas, P. Wienberger, L. Szunyogh, *et al.*, Phys. Rev. B **60**, 492 (1999).
12. H. Hasegawa, Phys. Rev. B **42**, 2368 (1990); **43**, 10803 (1991); **47**, 15073 (1993).
13. S. Zhang, P. M. Levy, and A. Fert, Phys. Rev. B **45**, 8689 (1992).
14. W. H. Butler, X.-G. Zhang, T. C. Shulthess, *et al.*, Phys. Rev. B **56**, 14574 (1997).
15. A. Vedyaev, N. Ryzhanova, B. Dieny, *et al.*, Phys. Rev. B **55**, 3728 (1997).
16. R. E. Camley and J. Barnas, Phys. Rev. Lett. **63**, 664 (1989).
17. J. Barnas, A. Fuss, R. E. Camley, *et al.*, Phys. Rev. B **42**, 8110 (1990); J. Magn. Magn. Mater. **140–144**, 497 (1995).
18. R. Q. Hood and L. M. Falicov, Phys. Rev. B **46**, 8287 (1992).
19. L. Sheng, D. Y. Xing, Z. D. Wang, and J. Dong, Phys. Rev. B **55**, 5908 (1997); **58**, 6428 (1998).
20. K. Majamdar, J. Chen, and S. Hershffeld, Phys. Rev. B **57**, 2950 (1998).
21. K. Fuchs, Proc. Cambridge Philos. Soc. **34**, 100 (1938).
22. H. Sondheimer, Adv. Phys. **1**, 1 (1952).
23. S. Zhang and P. M. Levy, Phys. Rev. B **57**, 5336 (1998).
24. V. Ya. Kravchenko, Zh. Éksp. Teor. Fiz. (in press).
25. D. A. Papaconstantopoulos, *Handbook of the Band Structure of Elemental Solids* (Plenum, New York, 1986).
26. W. F. Egelhoff, Jr., T. Ha, R. D. K. Misra, *et al.*, J. Appl. Phys. **78**, 273 (1995).
27. H. J. W. Swagten, G. J. Strijker, P. J. H. Bloemen, *et al.*, Phys. Rev. B **53**, 9108 (1996).
28. C. T. Yu, K. Westerholt, K. Theis-Brohl, *et al.*, Phys. Rev. B **57**, 2955 (1998).
29. V. Sato, S. Ishio, and T. Miyazaki, IEEE Transl. J. Magn. Jpn. **9**, 44 (1994).
30. S. Li, C. Yu, W. Lai, *et al.*, J. Appl. Phys. **78**, 405 (1995).

Translated by E. Golyamina

JETP Letters, Vol. 74, No. 8, 2001, pp. 431–435. From Pis'ma v Zhurnal Éksperimental'noĭ i Teoreticheskoĭ Fiziki, Vol. 74, No. 8, 2001, pp. 472–476.

Magnetic Polarons (Ferrons) of Complicated Structure[1]

E. L. Nagaev

Institute of Radioengineering and Electronics, Russian Academy of Sciences, Moscow, 101999 Russia
e-mail: tsir@elch.chem.msu

Received September 18, 2001; in final form, September 25, 2001

So far, magnetic polarons in antiferromagnetic semiconductors (ferrons) were assumed to arise due to the charge carrier self-trapping by a ferromagnetic or canted antiferromagnetic region. If the ferron size is not very large, they should have much more complicated structure: the magnetically deformed region consists not only of a magnetized core, which traps the electron, but also of its surrounding with the oppositely directed total moment, which repulses the trapped electron. The compensating moment of the surrounding oscillates with a period of the doubled lattice constant and with the amplitude diminishing very smoothly on an increase in the distance from the core. © *2001 MAIK "Nauka/Interperiodica".*

PACS numbers: 75.30.-m; 75.50.Pp

The energy of a charge carrier in a magnetic semiconductor depends strongly on the type of magnetic ordering, being minimal for the ferromagnetic ordering. For this reason the carriers tend to establish the latter. In nondegenerate antiferromagnetic semiconductors, they can do this only inside a small region, since a single electron cannot establish a ferromagnetic ordering in a crystal of macroscopic size. The idea that a mobile electron or hole creates a magnetized region inside of an antiferromagnetic semiconductor, which traps it, was advanced more than 30 years ago [1–4], and later was used by many other authors (see, e.g., the review article [5]). In its simplest version, a conduction electron creates a ferromagnetic region and stabilizes it by its localization inside this region.

Certainly, this state belongs to the self-trapped ones and, in this respect, resembles the well-known lattice polaron. This justifies, to some extent, the use of the name "magnetic polaron," which it adopted in the pioneering papers [1, 2]. But, in reality, this name is inaccurate, as the creation of this quasiparticle means a change of the crystal magnetization. Meanwhile, the term "magnetic polarization" is never used for the crystal magnetization. For this reason, I later proposed the name "ferron" for the quasiparticle invented by me in [1, 2]. The ferrons were observed experimentally in EuSe and EuTe [6].

In addition to the free ferrons, the bound ferrons were considered in [2, 7, 8]. They correspond to the electrons (holes) captured by the donor (acceptor) impurities in antiferromagnetic semiconductors. These electrons (holes) produce magnetized regions in the vicinity of the donors, which attract the electrons to donors, jointly with the Coulomb potential of the donor atom. The central portion of the magnetized region may be completely ferromagnetic, and the rest may be canted antiferromagnetic. Perhaps, the former may be absent. The bound ferrons strongly influence the electrical and magnetic properties of the crystals. In particular, due to their large magnetic moments, bound ferrons can change the sign of the paramagnetic Curie temperature from negative to positive. They also lead to a jump in the crystal magnetization in weak magnetic fields [9].

These results were obtained for the ferron sizes larger than the lattice constant. In this paper, the ferrons whose size is comparable with that of the lattice constant will be considered. It will be shown that, in some cases, its structure may be considerably more complicated than that of the large ferrons. Especially nontrivial is the fact that the local magnetization can have alternating signs. This means that the core of the magnetically deformed region attracts the electron, and the region outside the core repulses it. The coordinate dependence of the compensating moment of the surrounding should be rather complicated for small magnetic anisotropy: it should oscillate with a period of doubled lattice constant and with the amplitude diminishing very smoothly upon an increase in the distance from the core.

Such a complex ferron can be considered the manifestation of a real magnetic polaron. In fact, the magnetic polarization corresponds to the appearance of a magnetic moment inside a certain region of the crystal and of a compensating moment with the opposite direction elsewhere. A close analogy with the lattice polarization is obvious. The latter leads to the appearance of the local charge density, but the total crystal charge remains zero. One should point out, however, that the total magnetization remains nonzero in the case considered, since the magnetic compensation is incomplete.

[1] This work was submitted by the author in English.

Hence, the quasiparticle discussed is intermediate between the ferron and the true magnetic polaron.

A simple model will be used to corroborate the idea of true magnetopolaronic effect. The self-trapped state, which is found in this model, corresponds to a state intermediate between the bound ferron and the bound true magnetic polaron. Due to an impurity potential, the electron is located at magnetic atoms closest to the impurity. The localization region acquires a core magnetic moment, becoming ferromagnetic or canted antiferromagnetic.

It will be shown that the region surrounding the localization region also acquires a magnetic moment. Its total value is opposite to the direction of the ferron moment and compensates the former by more than 70% in the one-dimensional case and by 40% in the three-dimensional case. The compensating moment displays oscillations with a period equal to the doubled lattice constant. If the magnetic anisotropy is small, the oscillation amplitude tends toward zero very smoothly. For larger anisotropy, the tendency toward the oscillation attenuation increases strongly. The magnetization compensation decreases the energy of the self-trapped state very strongly, e.g., more than twice in the one-dimensional case.

First, a one-dimensional chain of magnetic atoms will be considered within the framework of the *s–d* model, to which the uniaxial magnetic anisotropy term is added, since it determines the direction of magnetic moments.

The atomic chain is directed along the *y* axis, and the magnetic easy axis is *x*. The undisturbed magnetic structure is represented by two sublattices with the spins up ($S^x = S$) for the even atomic numbers $g = 2n$ and spins down ($S^x = -S$) for the odd atomic numbers $g = 2n + 1$. Under the influence of the trapped electron, the *d* spins can be deviated from the *x* axis. The donor impurity is assumed to be located symmetrically about these two atoms belonging to different magnetic sublattices. Then the Hamiltonian of the system can be represented in the form

$$H_{sd} = -t[a^*_{-1,\sigma}a_{0,\sigma} + a^*_{0,\sigma}a_{-1,\sigma}] - A\sum_{g=-1,0}(\mathbf{s}\mathbf{S}_g)_{\sigma\sigma'}a^*_{g,\sigma}a_{g,\sigma'} - I\sum\mathbf{S}_g\mathbf{S}_{g+1} - K\sum(S^x_g)^2, \quad (1)$$

where $a^*_{g,\sigma}$, $a_{g,\sigma}$ are the *s*-electron operators corresponding to the conduction electrons or holes at atom *g* with the spin projection σ; $\mathbf{s}$ is the *s*-electron spin operator; and $\mathbf{S}_g$ is that of the *d*-spin of atom *g*, the *d* spin magnitude being *S*. The form (1) assumes that the *d–d*-exchange integral *I* corresponding to the antiferromagnetic ordering is negative. The constant *K* of the uniaxial anisotropy is positive. The energy of the Coulomb interaction between the impurity and the electron is an additive constant and, for this reason, is omitted here.

Only the lowest bound state of the conduction electron will be considered. It corresponds to the *s* electron shared with equal probabilities between atoms with the numbers $g = -1$ and $g = 0$. Perhaps, such a situation is possible also for the self-trapped electron in a perfect crystal but for very special parameter values.

We begin with the case of the magnetic anisotropy tending toward zero. The electron effect on the *d* spins is tantamount to an effective magnetic field directed along the *z* axis. Hence, in the vicinity of the impurity, the *d* spins lie inside the *z–x* plane. By the symmetry of the system with $K \longrightarrow 0$, $S^z_{2n} = S^z_{-2n-1}$ with the magnetized core formed by atoms –1 and 0, and the S^x components are of the opposite signs for the two sublattices.

In what follows, the inequality $AS \ll W$ will be used first, where *W* is the charge-carrier bandwidth. In this case, it is convenient to carry out the canonical transformation of the *s*-electron operators, which diagonalizes the first term in Eq. (1):

$$a_{\pm,\sigma} = 2^{-1/2}[a_{-1,\sigma} \pm a_{0,\sigma}]. \quad (2)$$

Then the standard procedure of constructing the magnetic Hamiltonian from the *s–d* Hamiltonian (1) can be used: the latter is averaged over the *s* electronic state. Taking its spin to be aligned with the *z*-axis, one puts $\langle a^*_{g,1/2}a_{g,1/2}\rangle = 1$ for $g = 0$ or –1 and all other averaged pairs of operators equal to zero.

Introducing the polar angles for the *d* spins, one can represent the magnetic energy in the form

$$E = J\sum_g\cos(\theta_g + \theta_{g+1}) - L[\cos\theta_{-1} + \cos\theta_0] + K/2\sum_g\sin^2\theta_g + E_0, \quad J = -IS^2, \quad L = AS/4, \quad (3)$$

where E_0 is the energy of the antiferromagnetic ordering. Minimizing Eq. (3) with respect to the polar angles of the spins θ_g, one obtains the following set of nonlinear equations:

$$J\sin(\theta_g + \theta_{g+1}) + J\sin(\theta_g + \theta_{g-1}) - L\sin\theta_g[\delta_{g,-1} + \delta_{g,0}] + K\sin(2\theta_g) = 0. \quad (4)$$

Obviously,

$$\theta_{\pm\infty} = \pi/2. \quad (5)$$

This boundary condition remains in force if $KS^2N \gg L$, where *N* is the number of atoms in the chain.

Further, the solution should satisfy the equality

$$\theta_{-(g+1)} = \theta_g \quad (6)$$

with $g \geq 0$. Hence, it is sufficient to consider nonnegative *g*.

The corresponding treatment for the double exchange case $W \ll AS$ can be carried out using the de Gennes [10] expression for the effective hopping integral between atoms 0 and (–1)

$$t_{\text{eff}} = t\cos\left(\frac{\theta_{-1} + \theta_0}{2}\right). \quad (7)$$

This equation ensures a high accuracy if the total angle between the spins is not very large [9]. Using Eqs. (1), (6), and (7), one again arrives at the set of Eqs. (4), but with $L = t$ in this case.

To solve the set of Eqs. (4), one should make it finite, putting

$$\theta_f = \pi/2 \quad (5a)$$

for some value f of the number of the atom. The cutoff of the set of Eqs. (4) at a finite f is equivalent to using a variational procedure. Hence, it exaggerates the energy, the smaller f the stronger exaggeration.

The case of $f = 1$ corresponds to the purely ferron state, where the magnetized region coincides with the core region, inside which the electron is localized (atoms 0 and –1). But already allowing for the deviation of the next spin ($f = 2$) will lead to the appearance of the magnetic polarization.

For $f = 2$, one can obtain solutions analytically if $L \ll 1$ or $L \gg 1$ (L in J units). In the former case, putting $\theta_0 = \pi/2 - \alpha$ and $\theta_1 = \pi/2 - \beta$, one finds for $KS^2 \ll L, J$: $\alpha = 2L/5$ and $\beta = -\alpha/2$. As the angles α and β are proportional to the core moment and to the compensating moment, respectively, one sees that the latter amounts to one half of the former. In the limiting case of large L, where $\theta_0 \ll 1$, one finds θ_1 to be $3\pi/4$. Hence, the compensating moment depends on L very weakly and amounts to 71% of the core moment.

Now let us discuss the intermediate L values. Results for them are obtained by numerical calculations based on the set of Eqs. (4). For example, for $L = 3$ the ground-state energies of the system in J units are –2.72 for $f = 1$, –4.78 for $f = 2$, and –5.846 for $f = 16$. Hence, even the simplest version of allowing for the compensating moment $f = 2$ decreases the bound ferron energy by a factor of 1.76, and for $f = 16$ by a factor of 2.15.

For $f = 1$, the ferron magnetic moment coinciding with that of the core (0 and –1 atoms) is $1.62S$. For $f = 2$, the core moment is $1.796S$, i.e., higher than for $f = 1$. But, instead, the compensating magnetic moment appears at atoms $g = 1$ and –2. Its total value is $-1.058S$, which amounts to 59% of the core moment. Hence, the total magnetic moment of the system is $0.738S$, which amounts only to 41% of the core magnetic moment.

But a more detailed investigation with $f = 16$ shows that the compensating magnetization is not concentrated in the closest vicinity to the core. It is long-range and has a rather complicated structure. To begin with, the total core moment is $1.992S$ for $L = 3$. Moreover, the same sublattice, to which the atom $g = 0$ belongs, is magnetized in the same direction as this atom, and the magnetization of the lattice decreases very smoothly, so that the magnetization of the atom $g = 14$ amounts to 18% of that of atom $g = 0$. But the other sublattice is magnetized still more strongly in the opposite direction, and this magnetization drops also very smoothly. Hence, the magnetization outside the ferron oscillates with a period of the doubled lattice constant and with the amplitude decreasing with increasing distance from the ferron (figure). The total compensating moment outside the electron localization region up to atom $g = 15$ is $-1.044S$.

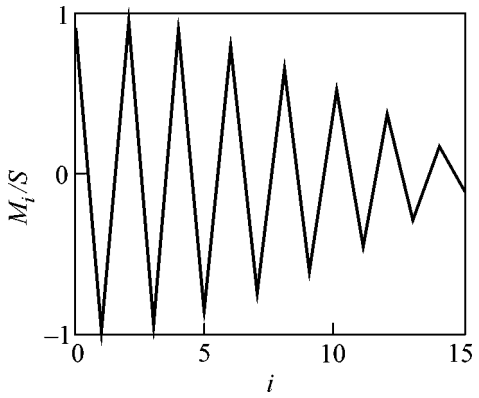

Dependence of the moment M_i on the number i of the magnetic atom (one-dimensional system).

The oscillation length decreases with increasing magnetic anisotropy. The fact that the anisotropy suppresses the magnetization oscillations is obvious from the limiting case of the Ising model $K \longrightarrow \infty$. Then, the magnetization is aligned not with the z axis but with the x axis. This problem is solved exactly: for $L < 2J$, the ferron does not exist, and for $L > 2J$ it corresponds to the spins of atoms 0 and (–1) parallel to each other. Outside this core the d spins form the ideal antiferromagnetic ordering, with the spins of atoms bordering the core being antiparallel to the core spin. Thus, the oscillations of the magnetic moment outside the core are really absent in the limit of a giant magnetic anisotropy.

The lower bound for the compensating moment amounts to 52% of the core moment. It should be noted that, though the energies for $f = 2$ and $f = 16$ differ only by 22%, qualitatively, the behaviors of the magnetic polarizations in these cases differ drastically.

Nevertheless, in both these cases the real contribution of such bound ferrons to the magnetization of the crystal in a magnetic field is considerably less than it was assumed initially. Hence, allowing for the magnetic polarization is necessary for the accurate calculation of the magnetic properties of the ferron-containing crystals.

The ferron contribution will be evaluated in the three-dimensional case. It will be assumed that the crystal structure is simple cubic, and that the antiferro-

magnetic ordering is staggered. The donor atom is located at the center of a unit cell, and the donor electron is spread over eight atoms located at the corners of the unit cell. Only the magnetic moments of these atoms and of 24 atoms adjacent to them will be taken into account. The former atoms form the moment of the ferron core M_C, and the latter, the compensating moment of the surrounding M_S.

Using the three-dimensional analogue of the Hamiltonian (1) and again introducing the angles θ_0 and θ_1 for the moments of the former and of the latter atoms, respectively, after minimizing the total energy with respect to the angles, one arrives at the following equations:

$$\begin{aligned} -3J\sin(2\theta_0) - 3J\sin(\theta_0 + \theta_1) + L\sin\theta_0 &= 0, \\ \sin(\theta_0 + \theta_1) + \sin(2\theta_1) + 3\cos\theta_1 &= 0. \end{aligned} \tag{8}$$

The solution to Eqs. (8) shows that the ratio M_S/M_C depends on L very weakly and is close to 40%. For the same reasons as in the one-dimensional case, the oscillations of the magnetic moment should also exist in the three-dimensional case. Again, the bound ferron-magnetic polaron energy is, by the order of magnitude, one-hundred percent lower than the ferron energy. This energy lowering is very large and points to a considerably smaller density of the thermally delocalized charge carriers than in the usual ferron scenario.

The energy of the ready-made noninteracting magnetic moments directed normally to the sublattice does not change upon their reversal. Hence, these moments can lead to a very rapid growth of the magnetization of the crystal in very small magnetic fields, with which they are aligned. It dominates for noticeable impurity densities, because the magnetization of the antiferromagnetic portion of the crystal is still very small in such fields. In the limiting case $T \longrightarrow 0$, an arbitrarily small field should cause a complete ordering of the bound ferron moments, which manifests itself as a steep jump in the magnetization of the crystal. As follows from the results presented above, this jump may turn out to be considerably less than it was assumed previously. At finite temperatures, if the field is too small to change the magnetic moments of the bound ferrons, the ferron contribution to the crystal magnetization is described by the Langevin function. Accordingly, the growth of this contribution with field turns out to be considerably more smooth.

It should be specially noted that the present investigation refutes the point of view expressed by some physicists, according to which the bound electrons can produce the canted antiferromagnetic ordering in antiferromagnetic semiconductors.

Concerning the actuality of the present investigation, it should be noted that the problem of magnetic polarons (ferrons) has remained actual for more than 30 years, beginning from their theoretical prediction [1]. This is related to the fact that ferrons determine the electrical and magnetic properties of many magnetic materials, including manganites, which attract much attention due to their giant magnetoresistance. At present, the existence of bound ferrons is beyond any doubt. Experimental data on them are presented in review article [11]. A refined theory of the ferron states developed in this work, which is based on the partial compensation of the magnetic moment of the ferromagnetic region by its surrounding, will make it possible to treat phenomena in these materials more consistently.

The theoretical prediction about the magnetization oscillations made above has not yet been confirmed by experiment, but this theoretical result is quite new and, possibly, will stimulate new experimental investigations. At least, this effect seems to be interesting from the physical point of view.

The small magnetic polarons investigated in this work are typical of weakly doped manganites, but they differ drastically from the small lattice polarons. The latter are characterized by the fact that, in the zeroth approximation, the electrons are localized at certain sites and, due to this, cannot establish the ferromagnetic ordering even in very small crystal regions (to do this, electron transitions between the magnetic atoms are necessary). The small magnetic polarons considered in this work allow the electron transitions between the magnetic atoms and, hence, the local ferromagnetic ordering.

It should be stressed that the small lattice polarons are hypothetical quasiparticles, and their existence has not seen proved yet. According to my estimates, the standard polarization small polarons are impossible in magnetic semiconductors and manganites, because they are only partially polar crystals [11, 12]. On the other hand, in the Jahn–Teller materials, such as manganites, the coupling strength between the holes and Jahn–Teller phonons is unknown. Meanwhile, this coupling should be very strong for the formation of small Jahn–Teller polarons, the reasons for which are not obvious.

The most decisive argument against small lattice polarons of both types in manganites is their metallic state at sufficiently high doping levels. Actually, in materials where they exist, Mott delocalization of the donor electrons or acceptor holes, i.e. the metallic state, is impossible because of giant effective masses of the charge carriers in the small-polaron states [11]. Again, the similarity of the basic properties of manganites with the properties of the standard non-Jahn–Teller and only partially polar magnetic semiconductors makes it possible to conclude that the small lattice polarons do not exist in manganites.

This work was supported in part by the Russian Foundation for Basic Research (project no. 01-02-97010), INTAS (grant no. 97-open-30253), and the Russian Ministry of Science and Industry.

REFERENCES

1. E. L. Nagaev, Pis'ma Zh. Éksp. Teor. Fiz. **6**, 484 (1968) [JETP Lett. **6**, 18 (1967)].
2. E. L. Nagaev, Zh. Éksp. Teor. Fiz. **54**, 228 (1968) [Sov. Phys. JETP **27**, 122 (1968)].
3. N. Mott and Z. Zinamon, Rep. Prog. Phys. **33**, 81 (1970).
4. N. F. Mott and E. A. Davis, *Electronic Processes in Non-Crystalline Materials* (Clarendon, Oxford, 1971; Mir, Moscow, 1974).
5. E. L. Nagaev, J. Magn. Magn. Mater. **110**, 39 (1992).
6. P. Wachter, CRC Crit. Rev. Solid State Sci. **3**, 189 (1972).
7. E. L. Nagaev, Phys. Rev. B **60**, 455 (1999).
8. E. L. Nagaev, Fiz. Tverd. Tela (St. Petersburg) **43**, 54 (2001) [Phys. Solid State **43**, 54 (2001)].
9. E. L. Nagaev, *Physics of Magnetic Semiconductors* (Nauka, Moscow, 1979; Mir, Moscow, 1983).
10. P. de Gennes, Phys. Rev. **118**, 141 (1960).
11. E. L. Nagaev, Phys. Rep. **346**, 388 (2001).
12. E. L. Nagaev, Phys. Rev. Lett. **84**, 2042 (2000).

JETP Letters, Vol. 74, No. 8, 2001, pp. 436–441. Translated from Pis'ma v Zhurnal Éksperimental'noĭ i Teoreticheskoĭ Fiziki, Vol. 74, No. 8, 2001, pp. 477–482.

On the Lorentz-Invariant Time–Energy Uncertainty Relation for a Relativistic Photon

S. N. Molotkov

Institute of Solid-State Physics, Russian Academy of Sciences, Chernogolovka, Moscow region, 142432 Russia

Received September 5, 2001

The time–energy uncertainty relation is discussed for a relativistic massless particle. The Lorentz-invariant uncertainty relation is obtained between the root-mean-square energy deviation and the scatter of registration time. The interconnection between this uncertainty relation and its classical analogue is established. © *2001 MAIK "Nauka/Interperiodica".*

PACS numbers: 03.65.Ta; 03.65.Ca

The notion of time–energy uncertainty relation

$$\overline{(\Delta\varepsilon)^2}\,\overline{(\Delta t)^2} \geq 1/4 \qquad (1)$$

in nonrelativistic quantum mechanics is not so well-defined as the other relations of this type, e.g., the coordinate–momentum uncertainty relation [1–4]. This is primarily caused by the fact that time is not a dynamical variable corresponding to a certain Hermitian operator, but is a parameter. Because of the presence of a lower bound in the spectrum of the Hamiltonian, one generally cannot introduce the Hermitian time operator [5]. The time–energy uncertainty relation was discussed in many works for a great variety of situations. For instance, in [6] the time–energy relation was derived for the internal evolution of a quantum system, but it did not describe the measurement process. A Hamiltonian allowing the instantaneous (in a time as short as one likes), exact, and reproducible energy measurement for a quantum system was written in [7]. True enough, no example of a physical system is known so far to which this Hamiltonian could be applied. In [7], the fact was used that external classical fields of a duration as short as one likes and an intensity as high as one likes are allowed by the formal apparatus of nonrelativistic quantum mechanics. This approach has come under criticism in [8]. For the relativistic case, the restrictions placed by special relativity on the measurability of quantum states were first discussed in [9]. Further inquiry was undertaken in [10]. It turned out that, strictly speaking, only the classical fields (potentials) can be treated classically in the Hamiltonian. The time-dependent fields require the quantum approach. Hence, the question of exact and reproducible energy measurement in a time as short as one likes was, in fact, merely reformulated in different terms.

Although time is not a dynamical variable, the measurement of event time is a rather routine experimental situation [11]. Let the event time be fixed experimentally; in this case, the registration time is a space of results. The interrelation between the probability distribution on the space of results (registration time) and the state of the quantum system is specified by a positive operator-valued measure. More precisely, to every subset $\Delta_t \in (-\infty, \infty)$ of the space of results, there is a positive operator $\mathcal{M}(\Delta_t)$ such that

$$\mathcal{M}(\cup\Delta_{it}) = \sum_i \mathcal{M}(\Delta_{it}), \quad \Delta_{it} \cap \Delta_{jt} = \varnothing. \qquad (2)$$

The normalization condition is that the total probability of events occurring over all space of results is unity:

$$\mathcal{M}(\Delta_{(-\infty,\,\infty)}) = I, \quad \Delta_{(-\infty,\,\infty)} \equiv (-\infty, \infty). \qquad (3)$$

In addition, the operator-valued measure in the expansion of unity (2) must satisfy the covariance condition. In the preparation of quantum state, the shifts in time origin must lead to corresponding shifts in the probability distribution; one has

$$\hat{U}_{t_0}\mathcal{M}(\Delta_t)\hat{U}_{t_0}^{-1} = \mathcal{M}(\Delta_{t-t_0}), \qquad (4)$$

where $\hat{U}_t$ is the evolution (time shift) operator.

One can introduce the most symmetric time operator

$$\hat{t} = \int_{-\infty}^{\infty} t\mathcal{M}(t, dt). \qquad (5)$$

The mean registration time is given by the standard expression

$$\bar{t} = \int_{-\infty}^{\infty} t\mathrm{Tr}\{\mathcal{M}(t, dt)\rho\}, \qquad (6)$$

where ρ is the density matrix of a quantum system subjected to measurement.

0021-3640/01/7408-0436$21.00

Accordingly, the root-mean-square deviation of registration time is defined as

$$\overline{(\Delta t)^2} = \int_{-\infty}^{\infty} (t - \bar{t})^2 \mathrm{Tr}\{\mathcal{M}(t, dt)\rho\}. \quad (7)$$

If H is the Hamiltonian of the system, then its spectral representation is

$$\hat{H} = \int_0^{\infty} \varepsilon \mathcal{E}(\varepsilon, d\varepsilon), \quad (8)$$

where $\mathcal{E}(\varepsilon, d\varepsilon)$ is the spectral family of orthogonal projectors. Note that the operator-valued measures $\mathcal{M}(t, dt)$ in Eq. (2) are not orthogonal.

The mean energy and the root-mean-square deviation are defined for the system in quantum state ρ as

$$\bar{\varepsilon} = \int_0^{\infty} \varepsilon \mathrm{Tr}\{\mathcal{E}(\varepsilon, d\varepsilon)\rho\}, \quad (9)$$

$$\overline{(\Delta\varepsilon)^2} = \int_0^{\infty} (\varepsilon - \bar{\varepsilon})^2 \mathrm{Tr}\{\mathcal{E}(\varepsilon, d\varepsilon)\rho\}. \quad (10)$$

Next, one may raise the question as to the attainable lower bound of the time–energy uncertainty relation, i.e., what are the quantum states for which the functional

$$\Omega = \min_{\{\rho\}} \{\overline{(\Delta\varepsilon)^2}\,\overline{(\Delta t)^2}\} \quad (11)$$

reaches its minimum?

Below, the time–energy relation in the sense given by Eqs. (2)–(11) is considered for a one-dimensional massless relativistic particle (photon). Although being a model, this example, nevertheless, encompasses all main features of the problem. Moreover, experiments with photons, as a rule, are carried out in one-dimensional optofiber systems.

Inasmuch as time is not an absolute category in the relativistic case, the notion of the time–energy uncertainty relation, at first glance, is defined even worse than in the nonrelativistic case. However, the distinctive feature of a photon is that its momentum and energy are linearly related to each other. Moreover, since the mass surface of a massless field coincides with the leading part of the light cone in momentum representation, all events for the states propagating in one direction occur at the light cone in the Minkowski space–time. As a result, the time–energy uncertainty relation becomes Lorentz-invariant (independent of the inertial coordinate system where the measurement is carried out). The lower bound in inequality (1) becomes slightly higher than 1/4.

Despite the fact that time is not an absolute category in the relativistic case and that, in contrast to the nonrelativistic case, the notion of the state (wave function) at a given instant of time (i.e., strictly speaking, the Schrödinger representation) does not exist, the time–energy uncertainty relation in the sense of Eqs. (2)–(11) is well defined.

The states of a free quantized field (more precisely, the generalized eigenvectors) are generated by the action of field operators (generalized functions with operator values)

$$\varphi^+(\hat{x}) = \frac{1}{\sqrt{2\pi}} \int d\hat{k}\, \delta(\hat{k}^2)\theta(k_0) e^{i\hat{k}\hat{x}} a^+(\hat{k}),$$
$$\hat{k} = (k, k_0), \quad \hat{x} = (x, t), \quad (12)$$
$$\hat{k} = dk dk_0, \quad \hat{k}\hat{x} = kx - k_0 t$$

on the vacuum vector [12]. The creation and annihilation operators satisfy relations

$$[a^-(\hat{k}), a^+(\hat{k}')] = k_0 \delta(k - k'). \quad (13)$$

The field physical states $|\psi\rangle \in \mathcal{H}$ belonging to the Hilbert space of states are obtained by integrating the generalized operator functions together with basic functions $\psi(\hat{x}) \in \Omega(\hat{x})$ {the generalized eigenvectors $\varphi^+(\hat{x})|0\rangle \in \Omega^*(\hat{x})$ are continuous linear functionals on $\Omega(\hat{x})$, where $\Omega(\hat{x}) \subset \mathcal{H} \subset \Omega^*(\hat{x})$ is the equipped Hilbert space [13]}. One has

$$|\psi\rangle = \int d\hat{x}\, \psi(\hat{x}) \varphi^+(\hat{x})|0\rangle$$

$$= \int d\hat{k}\, \psi(\hat{k}) \delta(\hat{k}^2)\theta(k_0) a^+(\hat{k})|0\rangle = \int_{-\infty}^{\infty} \frac{dk}{k_0} \psi(k, k_0 = |k|)|\hat{k}\rangle,$$
$$|\hat{k}\rangle = a^+(\hat{k})|0\rangle, \quad \langle \hat{k}, \hat{k}' \rangle = k_0 \delta(k - k'), \quad (14)$$
$$\psi(\hat{k}) = \int d\hat{x}\, \psi(\hat{x}) e^{-i\hat{k}\hat{x}},$$

where dk/k_0 is the Lorentz-invariant integration volume.

The contribution to the physical state $|\psi\rangle$ comes from the amplitude $\psi(k, k_0 = |k|)$ at the mass surface (leading part of the light cone in momentum representation).

We consider the states propagating in one direction. For the states propagating in both directions, the notion of event time has no sense. For the states propagating in one direction (for definiteness, $k > 0$), energy and momentum are one and the same, because of the linear relationship between them, $k_0 = |k| = k$. For these states, only the vectors with $k > 0$ make a contribution to Eq. (14), and the amplitude $\psi(k, k)$ is nonzero at $k > 0$.

The energy (momentum) measurement is given by the expansion of unity in the subspace of one-particle states:

$$I = \int_{-\infty}^{\infty} \frac{dk}{k_0} |\hat{k}\rangle\langle\hat{k}| = \int_{-\infty}^{\infty} \mathcal{M}(k, dk),$$
$$\mathcal{M}(k, dk) = |\hat{k}\rangle\langle\hat{k}| \frac{dk}{k_0}, \quad I_+ = \int_0^{\infty} \mathcal{M}(k, dk). \tag{15}$$

In actuality, it will suffice to restrict oneself to the subspace of states projected onto the vectors $|\hat{k}\rangle$ with $k > 0$; I_+ is unity in this subspace. The probability of measuring energy (momentum) in the interval $(k, k + dk)$ is given by

$$\Pr\{dk\} = \mathrm{Tr}\{\mathcal{M}(k, dk)|\psi\rangle\langle\psi|\}$$
$$= |\psi(k, k)|^2 \frac{dk}{k} = |f(k)|^2 dk, \quad f(k) = \frac{\psi(k, k)}{\sqrt{k}}. \tag{16}$$

The mean energy (momentum) in the state $|\psi\rangle$ is

$$\bar{k} = \int_0^{\infty} k \Pr\{dk\} = \int_0^{\infty} k |f(k)|^2 dk, \tag{17}$$

and the root-mean-square deviation is

$$\overline{(\Delta k)^2} = \int_0^{\infty} (k - \bar{k})^2 \Pr\{dk\} = \overline{k^2} - (\bar{k})^2,$$
$$\overline{k^2} = \int_0^{\infty} k^2 \Pr\{dk\}. \tag{18}$$

Let us now consider the measurement of particle position; for the states propagating in one direction ($k > 0$), this position can be represented by the expansion of unity:

$$I_+ = \int_{-\infty}^{\infty} \frac{dx}{2\pi} \left(\int_0^{\infty} \frac{dk}{\sqrt{k}} e^{-i\hat{k}\hat{x}} |\hat{k}\rangle \right) \left(\int_0^{\infty} \frac{dk'}{\sqrt{k'}} \langle\hat{k}'| e^{i\hat{k}'\hat{x}} \right)$$
$$= \int_{-\infty}^{\infty} \frac{d\tau}{2\pi} \left(\int_0^{\infty} \frac{dk}{\sqrt{k}} e^{-ik\tau} |\hat{k}\rangle \right) \left(\int_0^{\infty} \frac{dk'}{\sqrt{k'}} \langle\hat{k}'| e^{ik'\tau} \right) = \int_{-\infty}^{\infty} \mathcal{M}(\tau, d\tau), \tag{19}$$

where $\tau = x - t$. The measurement of the coordinate x is, in fact, the measurement of response time t. More precisely, the space of results is formed not by x and t separately, but by their difference τ. The expansion of unity in Eq. (19) formally describes an instrument; it can be interpreted as follows. If the space of results is formed by x, then the measurement should be understood as an x-distributed instrument generating a random result at point $(x, x + dx)$ and time t. If x is fixed, then the measurement describes an x-localized instrument operating in a trigger mode and generating a result at a random instant of time $(t, t + dt)$. The fact that the operator-valued measure $\mathcal{M}(\tau, d\tau)$ in Eq. (19) depends only on the difference $\tau = x - t$ means that, if the result can be obtained at the point x at the time instant t with a certain probability, then the same result can be obtained at a different point x' with the same probability, but at the instant of time $t' = x' - x + t$.

Accordingly, the probability of obtaining the result at time interval $(\tau, \tau + \tau)$ is, by definition,

$$\Pr\{d\tau\} = \mathrm{Tr}\{\mathcal{M}(\tau, d\tau)|\psi\rangle\langle\psi|\} = |f(\tau)|^2 d\tau, \tag{20}$$

$$f(\tau) = \int_0^{\infty} \frac{dk}{\sqrt{k}} \psi(k, k) e^{-ik\tau}. \tag{21}$$

It is notable that $f(\tau)$ coincides with the Landau–Peierls wave function in coordinate representation [14]. Contrary to $\bar{k}$, the mean value of $\bar{\tau}$ can be chosen to be zero upon the appropriate choice of time origin. The root-mean-square deviation of registration time is

$$\overline{(\Delta\tau)^2} = \int_{-\infty}^{\infty} d\tau \Pr\{d\tau\} = \int_{-\infty}^{\infty} \tau^2 |f(\tau)|^2 d\tau$$
$$= \int_0^{\infty}\int_0^{\infty} dk\, dk'\, f(k) f^*(k') \int_{-\infty}^{\infty} \tau^2 e^{i(k-k')\tau} d\tau \tag{22}$$
$$= \int_0^{\infty}\int_0^{\infty} dk\, dk'\, f(k) f^*(k') \frac{\partial^2}{\partial k \partial k'} \delta(k - k') = \int_0^{\infty} \left| \frac{df(k)}{dk} \right|^2 dk.$$

The further goal consists of finding the state $|\psi\rangle$, for which the functional (11)

$$\Omega(f) = \left(\int_0^{\infty} \left| \frac{df(k)}{dk} \right|^2 dk \right) \left(\int_0^{\infty} (k^2 - \bar{k}^2) |f(k)|^2 dk \right) \tag{23}$$

is minimum under the additional normalization condition

$$\langle\psi|\psi\rangle = \int_0^{\infty} \frac{dk}{k} |\psi(k, k)|^2 = \int_0^{\infty} |f(k)|^2 dk = 1. \tag{24}$$

It turns out that the problem

$$\delta\Omega(f)/\delta f = 0 \tag{25}$$

of minimizing functional (23) was solved for classical signals in an elegant though little-known work [15] as early as 1934 (see also [16, 17]). It was shown that, for the time–frequency uncertainty relation as defined in Eq. (23), the functional reaches its minimum on even time functions $f(\tau)$ [accordingly, $df(k)/dk|_{k=0} = 0$]. The

corresponding variational problem reduces to the second-order differential equation for $f(k)$ of the form

$$\frac{d^2 f(x)}{dx^2} + \left(\nu + \frac{1}{2} - \frac{x^2}{4}\right) f(x) = 0,$$
$$x = \left(\frac{4a}{b - c^2}\right)^{1/4}(k - c), \quad \nu + \frac{1}{2} = \sqrt{a(b - c^2)}, \tag{26}$$

where

$$a = \int_0^\infty \left(\frac{df(k)^2}{dk}\right)^2 dk, \quad b = \int_0^\infty k^2 f(k)^2 dk,$$
$$c = \int_0^\infty k f(k)^2 dk, \quad \int_0^\infty f^2(k) dk = 1. \tag{27}$$

Here, the integrals a, b, and c are taken along the extremum. Taking into account that $df(k)/dk|_{k=0} = 0$ and that $b = 3c^2/2$ for the extremum, the solution is given by the parabolic cylinder function (Weber function) $D_\nu(x)$ [18]. The value of ν is determined from the condition $D'_\nu(x) = dD_\nu(x)/dx = 0$ at $k = 0$. Taking into account that

$$D_\nu(x) = \frac{e^{-x^2/4}}{\Gamma(-\nu)} \int_0^\infty e^{-x\xi - \xi^2/2} \xi^{-\nu - 1} d\xi, \tag{28}$$

this is equivalent to the solution of the transcendental equation

$$D'_{\mu - \frac{1}{2}}(-2\sqrt{\mu}) = 0,$$
$$\int_0^\infty e^{2\sqrt{\mu}\xi - \xi^2/2} \xi^{-\mu - 1/2} (\xi - \sqrt{\mu}) d\xi = 0, \tag{29}$$

where $\mu = \nu + 1/2$. The numerical value is given in [17]: $\mu^2 = 0.2951\ldots$. The functional in its extremum equals

$$\Omega_{\min}(f) = \frac{ab}{3} = \mu^2 = 0.2951. \tag{30}$$

Let us now show that these time–energy uncertainty relations are Lorentz-invariant, i.e., remain unchanged upon measuring quantum state in any inertial frame of reference. The measurements in the observer's frame of reference are also formulated as in Eqs. (15) and (19); in doing so, by all quantities in Eqs. (15) and (19) should be meant their values in the observer's frame of reference, while the state obtained by the action of the respective unitary operator of the Poincaré group representation should be taken as a quantum state "seen" by the observer in the moving coordinate system. The general coordinate transformation in the Poincaré group consists of the translation in the Minkowski space–time and the Lorentzian rotation; one has

$$\hat{x}' = \hat{P}(\hat{a})\hat{L}\hat{x} = \hat{L}\hat{x} + \hat{a}, \tag{31}$$

where $\hat{P}(\hat{a})$ is the operator of translation by $\hat{a} = (a, a_0)$ and $\hat{L}$ is the operator of Lorentzian rotation describing the transition to a different inertial system. These transformations induce operator transformations

$$\hat{\mathbf{U}}(\hat{L}, \hat{a}) a^+(\hat{k}) \hat{\mathbf{U}}^{-1}(\hat{L}, \hat{a}) = e^{i\hat{L}\hat{k}\hat{a}} a^+(\hat{L}\hat{k}), \tag{32}$$

where $\hat{\mathbf{U}}(\hat{L}, \hat{a})$ is the unitary operator acting in $\mathcal{H}$.

The transformed state effectively seen by the observer is

$$|\psi(\hat{L}, \hat{a})\rangle = \hat{\mathbf{U}}(\hat{L}, \hat{a})|\hat{\psi}\rangle$$
$$= \int d\hat{x}\psi(\hat{x})\hat{\mathbf{U}}(\hat{L}, \hat{a})\varphi^+(\hat{x})\hat{\mathbf{U}}(\hat{L}, \hat{a})^{-1}\hat{\mathbf{U}}(\hat{L}, \hat{a})|0\rangle$$
$$= \int d\hat{x}\psi(\hat{x})\varphi(\hat{L}\hat{x} + \hat{a})|0\rangle = \int d\hat{x}\psi(\hat{L}^{-1}(\hat{x} - \hat{a}))\varphi^+(\hat{x})|0\rangle$$
$$= \int d\hat{k}\psi(\hat{k}) e^{i\hat{k}\hat{a}} \delta(\hat{k}^2)\theta(k_0) a^+(\hat{L}\hat{k})|0\rangle \tag{33}$$
$$= \int d\hat{k}\psi(\hat{L}^{-1}\hat{k}) e^{i\hat{k}\hat{a}} |\hat{k}\rangle = \int_0^\infty \frac{dk}{k} \psi(\hat{L}^{-1}\hat{k}) e^{i\hat{k}\hat{a}} |\hat{k}\rangle$$
$$= \int_0^\infty \frac{dk}{k} \psi\left(\frac{k - \beta k_0}{\sqrt{1 - \beta^2}}, \frac{k_0 - \beta k}{\sqrt{1 - \beta^2}}\right) e^{i(ka - k_0 a_0)} |\hat{k}\rangle,$$

where dk/k_0 is the Lorentz-invariant volume of integration. In Eq. (33), the invariance of the vacuum vector, $\hat{\mathbf{U}}(\hat{L}, \hat{a})|0\rangle = |0\rangle$, is also taken into account. Recall that only those states are considered which propagate in one direction along the x axis. The final state seen by the observer is written as

$$|\psi(\hat{L}, \hat{a})\rangle = \int_0^\infty \frac{dk}{k} \psi\left(k\sqrt{\frac{1 - \beta}{1 + \beta}}, k\sqrt{\frac{1 - \beta}{1 + \beta}}\right) |\hat{k}\rangle. \tag{34}$$

The mean energy (momentum) measured by the observer is defined as (the quantities in the moving coordinate system are labeled m)

$$\overline{k_m} = \int_0^\infty k \Pr\{dk\}$$
$$= \int_0^\infty k \mathrm{Tr}\{\mathcal{M}(k, dk)|\psi(\hat{L}, \hat{a})\rangle\langle\psi(\hat{L}, \hat{a})|\} \tag{35}$$
$$= \int_0^\infty \frac{dk}{k} k \left|\psi\left(k\sqrt{\frac{1 - \beta}{1 + \beta}}, k\sqrt{\frac{1 - \beta}{1 + \beta}}\right)\right|^2 = \bar{k}\sqrt{\frac{1 + \beta}{1 - \beta}}.$$

At small $\beta \ll 1$, the mean momentum (energy) in the moving system is related to its value in the fixed coordinate system by the expression

$$\overline{k_m} = \bar{k}(1+\beta) = k(1 - v/c), \tag{36}$$

which, in fact, is a formulation of the Doppler effect.

The respective energy (momentum) root-mean-square deviation in the moving coordinate system is

$$\overline{(\Delta k)_m^2} = \int_0^\infty (k - \overline{k_m})^2 \Pr\{dk\}$$

$$= \int_0^\infty (k - \overline{k_m})^2 \mathrm{Tr}\{\mathcal{M}(k, dk)|\psi(\hat{L}, \hat{a})\rangle\langle\psi(\hat{L}, \hat{a})|\} \tag{37}$$

$$= \int_0^\infty \frac{dk}{k}(k - \overline{k_m})^2 \left|\psi\left(k\sqrt{\frac{1-\beta}{1+\beta}}, k\sqrt{\frac{1-\beta}{1+\beta}}\right)\right|^2$$

$$= \left(\frac{1+\beta}{1-\beta}\right)\overline{(\Delta k)^2}.$$

The root-mean square deviation of registration time in the moving system is defined as (for the sake of convenience, the coordinate systems in this formula have the common origin, i.e., $\hat{a} = 0$, and only the Lorentzian rotation $\hat{L}$ is retained)

$$\overline{(\Delta\tau)_m^2} = \int_{-\infty}^\infty \tau^2 \Pr\{d\tau\}$$

$$= \int_{-\infty}^\infty \tau^2 \mathrm{Tr}\{\mathcal{M}(\tau, d\tau)|\psi(\hat{L}, \hat{0})\rangle\langle\psi(\hat{L}, \hat{0})|\}$$

$$= \int_{-\infty}^\infty \tau^2 \left|\int_0^\infty \frac{dk}{\sqrt{k}} e^{-ik\tau}\psi\left(k\sqrt{\frac{1-\beta}{1+\beta}}, k\sqrt{\frac{1-\beta}{1+\beta}}\right)\right|^2 \frac{d\tau}{2\pi} \tag{38}$$

$$= \int_{-\infty}^\infty \tau^2 \left|\int_0^\infty \frac{dk}{\sqrt{k}} \exp\left\{-ik\left(\tau\sqrt{\frac{1+\beta}{1-\beta}}\right)\right\}\psi(k, k)\right|^2$$

$$\times d\left(\frac{\tau}{2\pi}\sqrt{\frac{1+\beta}{1-\beta}}\right) = \overline{(\Delta\tau)^2}\left(\frac{1-\beta}{1+\beta}\right).$$

It follows from Eqs. (37) and (38) that the resulting time–energy uncertainty relation in the observer's moving coordinate system is related to the uncertainty relation in the initial system as

$$\overline{(\Delta k)_m^2}\,\overline{(\Delta\tau)_m^2} = \overline{(\Delta k)^2}\,\overline{(\Delta\tau)^2} = 0.2951\ldots > 1/4, \tag{39}$$

i.e., it is Lorentz-invariant.

The fact that the time–energy uncertainty relation is Lorentz-invariant is due, in fact, to the covariance of the energy (momentum) and event-time measurements. Indeed, the operator-valued measure in Eq. (19) is covariant about the Poincaré group transformations:

$$\hat{\mathbf{U}}(\hat{L}, \hat{a})\mathcal{M}(\tau, d\tau)\hat{\mathbf{U}}(\hat{L}, \hat{a})^{-1}$$

$$= \mathcal{M}\left(\sqrt{\frac{1-\beta}{1+\beta}}\tau - (a - a_0), d\left(\sqrt{\frac{1-\beta}{1+\beta}}\tau\right)\right). \tag{40}$$

The momentum measurement and the orthogonal operator measure in Eq. (15) also satisfy the covariance condition

$$\hat{\mathbf{U}}(\hat{L}, \hat{a})\mathcal{M}(k, dk)\hat{\mathbf{U}}(\hat{L}, \hat{a})^{-1}$$

$$= \mathcal{M}\left(\sqrt{\frac{1+\beta}{1-\beta}}k, d\left(\sqrt{\frac{1+\beta}{1-\beta}}k\right)\right). \tag{41}$$

If the measurement occurs in the same inertial coordinate system, $\hat{L} = \hat{1}$, then the covariance condition (41) is analogous to the nonrelativistic case (4), being the only difference the that the covariance is understood in the sense of translations in Minkowski space–time (in our case, shifts along the light cone branch).

I am grateful to S.S. Nazin for discussions and critical remarks. This work was supported by the projects "Physical Foundations of the Quantum Computer" and "Electronic States."

REFERENCES

1. W. Heisenberg, Z. Phys. **60**, 56 (1927).
2. N. Bohr, *Selected Scientific Works* (Nauka, Moscow, 1971), Vol. 2.
3. N. S. Krylov and V. A. Fok, Zh. Éksp. Teor. Fiz. **17**, 93 (1947).
4. E. P. Wigner, in *Aspects of Quantum Theory*, Ed. by A. Salam and E. P. Wigner (Cambridge Univ. Press, Cambridge, 1972), p. 237.
5. A. S. Holevo, *Probabilistic and Statistical Aspects of Quantum Theory* (North-Holland, Amsterdam, 1980).
6. L. I. Mandel'shtam and I. E. Tamm, Izv. Akad. Nauk SSSR, Ser. Fiz. **9**, 122 (1945).
7. Y. Aharonov and D. Bohm, Phys. Rev. **122**, 1649 (1961); Y. Aharonov and J. L. Safko, Ann. Phys. **91**, 279 (1975).
8. V. A. Fok, Zh. Éksp. Teor. Fiz. **42**, 1135 (1962) [Sov. Phys. JETP **15**, 784 (1962)].
9. L. D. Landau and R. Peierls, Z. Phys. **69**, 56 (1931); L. D. Landau, in *A Collection of Scientific Works* (Nauka, Moscow, 1969), Vol. 1, p. 56.
10. N. Bohr and L. Rosenfeld, Math.-Fys. Medd. **12**, 3 (1933); N. Bohr, *A Colection of Scientific Works* (Nauka, Moscow, 1971).
11. P. Busch, quant-ph/0105049; P. Busch, M. Grabowski, and P. J. Lahti, *Operational Quantum Physics* (Springer-Verlag, Berlin, 1995), Springer Lecture Notes in Physics, Vol. 31.

12. N. N. Bogolyubov, A. A. Logunov, A. I. Oksak, and I. T. Todorov, *General Principles of Quantum Field Theory* (Nauka, Moscow, 1987).

13. I. M. Gel'fand and N. Ya. Vilenkin, *Generalized Functions* (Fizmatgiz, Moscow, 1961; Academic, New York, 1964), Vol. 4.

14. L. D. Landau and R. Peierls, Z. Phys. **62**, 188 (1930); L. D. Landau, in *A Collection of Scientific Works* (Nauka, Moscow, 1969), Vol. 1, p. 56.

15. A. G. Maĭer and E. A. Leontovich, Dokl. Akad. Nauk SSSR **4**, 353 (1934).

16. A. A. Kharkevich, *Spectra and Analysis* (Fizmatgiz, Moscow, 1962).

17. V. V. Dodonov and V. I. Man'ko, in *Invariants and Evolution of Nonstationary Quantum Systems*, Ed. by M. A. Markov (Nauka, Moscow, 1987), Tr. Fiz. Inst. Akad. Nauk SSSR, Vol. 183.

18. *Heigher Transcendental Functions (Bateman Manuscript Project)*, Ed. by A. Erdelyi (McGraw-Hill, New York, 1953; Nauka, Moscow, 1966).

Translated by V. Sakun

JETP Letters, Vol. 74, No. 8, 2001, pp. 442.

ERRATA

Erratum: "Do Neutrino Oscillations Allow an Extra Phenomenological Parameter" [*JETP Letters* 73, no. 8, 380 (2001)]

I. S. Tsukerman

PACS numbers: 14.60.Pq; 12.15.Ff

In this paper, all references to formula numbers in the second column of the text are erroneous. One should read

(1) and (2) instead of (2) and (3),

(4)–(6) instead of (6)–(8),

(1) instead of (5),

(7) instead of (3),

(3) and (6) instead of (7) and (8).

The author and editorial board wish to apologize for this error.